ISA Transactions 58 (2015) 292–308

Contents lists available at ScienceDirect

ISA Transactions

journal homepage: www.elsevier.com/locate/isatrans

A novel auto-tuning PID control mechanism for nonlinear systems

Meric Cetin [a,*], Serdar Iplikci [b]

[a] Pamukkale University, Department of Computer Engineering, Kinikli Campus, 20070 Denizli, Turkey
[b] Pamukkale University, Department of Electrical and Electronics Engineering, Kinikli Campus, 20070 Denizli, Turkey

ARTICLE INFO

Article history:
Received 7 May 2014
Received in revised form
20 May 2015
Accepted 27 May 2015
Available online 24 June 2015
This paper was recommended for publication by Prof. A.B. Rad.

Keywords:
Model-based predictive control
Auto-tuning
PID controller
MIMO PID controller design
Real-time control

ABSTRACT

In this paper, a novel Runge–Kutta (RK) discretization-based model-predictive auto-tuning proportional-integral-derivative controller (RK-PID) is introduced for the control of continuous-time nonlinear systems. The parameters of the PID controller are tuned using RK model of the system through prediction error-square minimization where the predicted information of tracking error provides an enhanced tuning of the parameters. Based on the model-predictive control (MPC) approach, the proposed mechanism provides necessary PID parameter adaptations while generating additive correction terms to assist the initially inadequate PID controller. Efficiency of the proposed mechanism has been tested on two experimental real-time systems: an unstable single-input single-output (SISO) nonlinear magnetic-levitation system and a nonlinear multi-input multi-output (MIMO) liquid-level system. RK-PID has been compared to standard PID, standard nonlinear MPC (NMPC), RK-MPC and conventional sliding-mode control (SMC) methods in terms of control performance, robustness, computational complexity and design issue. The proposed mechanism exhibits acceptable tuning and control performance with very small steady-state tracking errors, and provides very short settling time for parameter convergence.

1. Introduction

Conventional PID controllers have been the most preferred controllers among others due to the simplicity of design and efficiency in the industrial applications and mechanical systems. The main problem about a PID controller is the fact that the parameters of the controller must be adjusted properly to satisfy a desired performance. For that purpose, many methods are proposed in the literature to tune PID parameters for linear time-invariant (LTI) systems [1–4]. Parameters of a PID controller must be tuned to provide satisfactory tracking of smooth reference signal of the linear time-varying (LTV) systems when the reference signal is variable. On the other hand, to design a PID controller for nonlinear systems, these parameters are usually tuned for local points using a linearization method. Linearization is mostly not satisfactory for all nonlinear systems due to the different linearization points and high nonlinearity. In addition, the structure of the system or reference point or environmental conditions may be changed or some internal or external disturbances may be involved in the control loop which cause different linearization points. All these circumstances lead to the necessity of one property of the PID controller: adaptation in the sense of auto-tuning. Therefore many PID controllers namely Sliding-mode (SM) adaptive PID controller for uncertain systems [5], neural-network (NN) based adaptive PID controller for the systems with unknown dynamics [6–9] and support-vector machine (SVM) based PID controller [10] have been proposed to tune PID parameters in the literature. Adaptive control scheme can be alternatively invoked a PID controller in cascade with fuzzy predictor [11]. Also, many new PID controllers which were tested for electromechanical systems are proposed in the literature [12–17].

Another popular control method namely Model Predictive Control (MPC) is used as advanced control technique in the literature. MPC-based controllers are preferred due to their advantages for linear/nonlinear system control such as handling of input and state constraints, accuracy and availability to control unstable, non-minimum phase and dead-time systems [18–21]. The design parameters, which are imposed by constraints of the system, must be large or small enough to assure nominal stability for MPC-based controllers [20]. In the constrained model-predictive control, the system must be taken away from one constraint to another. This is much more difficult for conventional structures such as PID or lead-lag compensator than MPCs. As a matter of fact, hybrid model predictive controllers have been very successful to solve such control problems. There are some studies related to hybrid MPCs. For example, to overcome stochastic disturbances and time delays, an internal model PID controller based on the Generalized Predictive Control (GPC) was developed

* Corresponding author. Tel.: +90 258 296 3208.
E-mail addresses: mcetin@pau.edu.tr (M. Cetin), iplikci@pau.edu.tr (S. Iplikci).

http://dx.doi.org/10.1016/j.isatra.2015.05.017
0019-0578/

in [22]. Afterwards, a different PID type controller which can be used for systems of any order based on the GPC was introduced [23]. As an other application of MPC in PID controller, the parameters of the PID are tuned with minimization of the objective function based on the CARIMA model of the systems as in [24,25]. Zhang et al. [26] proposed a novel PID controller optimized by extended non-minimal state space model predictive control framework for the temperature regulation. In [26], the proposed controller has combined the simple structure of the PID and good control performance of the MPC. In [27] Keyser et al. proposed a nonlinear extended prediction self-adaptive control (NEPSAC) mechanism which has used the nonlinear model for prediction. Other predictive control methods such as fuzzy predictive model with MPC have also been developed [28]. In the fuzzy predictive model, fuzzy control is used for controlling the uncertainty of the linear/nonlinear systems whose dynamics are unknown. In [29], a RK model-based predictive control, state and parameter estimation approach has been proposed, which inspired us to develop a robust, adaptive and predictive PID auto-tuning mechanism.

In this paper, a novel auto-tuning PID mechanism within the RK-MPC framework has been proposed for nonlinear systems. The mechanism provides some superior features in terms of control performance, robustness and design issues. In general, the proposed PID auto-tuning method includes three important characteristics: (i) robustness from the PID control structure, (ii) fast convergence from the MPC framework, (iii) adaptive behavior due to gradient-based adaptation, which constitute the main motivation of the paper. In addition to the introduction of a novel method, we have conducted two real-time control experiments on a SISO (unstable nonlinear MagLev system) and a MIMO (nonlinear three-tank liquid-level system) system. Moreover, the experimental studies include noisy and disturbance cases, and comparisons to control methods namely, standard PID, standard NMPC, RK-MPC [29] and standard SMC from the literature, which reinforces the contribution of the paper to the control theory literature.

The paper is organized as follows: Problem definition is explained in Section 2. Section 3 presents the proposed Runge–Kutta model-based PID controller structure. The real-time experimental results are shown in Section 4. The concluding remarks about the designed controller are presented in Section 5.

2. Problem statement

A nonlinear dynamical system is often expressed as the state and measurement equations. Consider an N-dimensional nonlinear continuous-time MIMO system:

$$\dot{\mathbf{x}} = \mathbf{f}(\mathbf{x},\mathbf{u}), \quad \mathbf{y} = \mathbf{g}(\mathbf{x},\mathbf{u}),$$
$$\mathbf{u} \in \mathbf{U}, \quad \mathbf{x} \in \boldsymbol{X}, \quad \forall t \geq 0. \tag{1}$$

where $\mathbf{x}(t) \in \Re^N$ is the state vector, $\mathbf{u}(t) \in \Re^R$ is the vector of control inputs and $\mathbf{y}(t) \in \Re^Q$ is the vector of output measurements. The state equations of the system are subject to state, input, input-slew and output constraints written as

$$X_i = \{x_i \in \Re |\ x_{i_{min}} \leq x_i \leq x_{i_{max}}, i = 1,\ldots,N\}$$
$$U_r = \{u_r \in \Re |\ u_{r_{min}} \leq u_r \leq u_{r_{max}}, r = 1,\ldots,R\}$$
$$\Delta U_r = \{\Delta u_r \in \Re |\ |\Delta u_r| \leq \Delta u_{r_{max}}, r = 1,\ldots,R\}$$
$$Y_q = \{y_q \in \Re |\ y_{q_{min}} \leq y_q \leq y_{q_{max}}, q = 1,\ldots,Q\}. \tag{2}$$

In order to use proposed RK-PID mechanism for the system, it is assumed that the functions $\mathbf{f}_i(.)$ $(i = 1,\ldots,N)$ and $\mathbf{g}_j(.)$ $(j = 1,\ldots,Q)$ are known and continuously differentiable with respect to the control inputs and the state variables. Also, it is assumed that the system is controllable. In this work, a novel RK model-based auto-tuning PID controller for nonlinear continuous-time system is presented. In this structure, a discretized model of the nonlinear system which is called the RK model [29] is obtained by the fourth-order RK algorithm and then utilized for the control of the systems. The RK model of the system is used for many purposes such as control, prediction, Jacobian calculation, parameter and state estimation [29,30]. The motivation behind the use of the fourth-order RK algorithm among others is the fact that it has been proved to be very accurate and stable [31,32].

2.1. Runge–Kutta discretization method

In this study, the well-known RK integration algorithm is adopted for obtaining the discretized models of the systems under investigation due to its higher accuracy and stability properties compared to other integration methods. For a given N-dimensional nonlinear continuous-time MIMO system as in (1), the current states $(x_1[n],\ldots,x_N[n])$ and the current inputs $(u_1[n],\ldots,u_R[n])$ of the system are given at the time index n where n denotes the sampling instant at $t = nT_s$. Now, the state vector and the output measurements of the system which belong to the next sampling time can be predicted by the fourth-order RK algorithm as follows: (initially, it is set $\hat{x}_1[n] = x_1(n),\ldots,\hat{x}_N[n] = x_N[n]$)

$$\begin{aligned}
&\hat{x}_1[n+1] = \hat{x}_1[n] + \tfrac{1}{6}(k_{11} + 2k_{12} + 2k_{13} + k_{14}),\\
&\vdots\\
&\hat{x}_N[n+1] = \hat{x}_N[n] + \tfrac{1}{6}(k_{N1} + 2k_{N2} + 2k_{N3} + k_{N4}),\\
&\hat{y}_1[n+1] = g_1(\hat{x}_1[n+1],\ldots,\hat{x}_N[n+1],u_1[n],\ldots,u_R[n])\\
&\vdots\\
&\hat{y}_Q[n+1] = g_Q(\hat{x}_1[n+1],\ldots,\hat{x}_N[n+1],u_1[n],\ldots,u_R[n])
\end{aligned} \tag{3}$$

where

$$\begin{aligned}
&k_{11} = T_s f_1(\hat{x}_1[n],\ldots,\hat{x}_N[n],u_1[n],\ldots,u_R[n]),\\
&\vdots\\
&k_{N1} = T_s f_N(\hat{x}_1[n],\ldots,\hat{x}_N[n],u_1[n],\ldots,u_R[n]),\\
&k_{12} = T_s f_1(\hat{x}_1[n]+0.5k_{11},\ldots,\hat{x}_N[n]+0.5k_{N1},u_1[n],\ldots,u_R[n]),\\
&\vdots\\
&k_{N2} = T_s f_N(\hat{x}_1[n]+0.5k_{11},\ldots,\hat{x}_N[n]+0.5k_{N1},u_1[n],\ldots,u_R[n]),\\
&k_{13} = T_s f_1(\hat{x}_1[n]+0.5k_{12},\ldots,\hat{x}_N[n]+0.5k_{N2},u_1[n],\ldots,u_R[n]),\\
&\vdots\\
&k_{N3} = T_s f_N(\hat{x}_1[n]+0.5k_{12},\ldots,\hat{x}_N[n]+0.5k_{N2},u_1[n],\ldots,u_R[n]),\\
&k_{14} = T_s f_1(\hat{x}_1[n]+k_{13},\ldots,\hat{x}_N[n]+k_{N3},u_1[n],\ldots,u_R[n]),\\
&\vdots\\
&k_{N4} = T_s f_N(\hat{x}_1[n]+k_{13},\ldots,\hat{x}_N[n]+k_{N3},u_1[n],\ldots,u_R[n]).
\end{aligned} \tag{4}$$

Eq. (3) can be organized as

$$\begin{aligned}
&\hat{\mathbf{x}}[n+1] = \hat{\mathbf{f}}(\hat{\mathbf{x}}[n],\mathbf{u}[n]) = \hat{\mathbf{x}}[n+1] + \mathbf{k}[n],\\
&\hat{\mathbf{y}}[n+1] = \mathbf{g}(\hat{\mathbf{x}}[n],\mathbf{u}[n]).
\end{aligned} \tag{5}$$

where

$$\mathbf{k}[n] = \frac{1}{6}\begin{bmatrix} k_{11}+2k_{12}+2k_{13}+k_{14} \\ k_{21}+2k_{22}+2k_{23}+k_{24} \\ \vdots \\ k_{N1}+2k_{N2}+2k_{N3}+k_{N4} \end{bmatrix} = \frac{1}{6}(\mathbf{k}_1 + 2\mathbf{k}_2 + 2\mathbf{k}_3 + \mathbf{k}_4) \tag{6}$$

Now, Eq. (5) associated with the discrete-time RK-model of a continuous-time system is available for RK model-based PID controller as explained in the next section in detail.

3. The proposed Runge–Kutta model-based PID controller

Although the structure proposed in this study aims at designing PID controllers for nonlinear systems, it should be kept in mind that the designed PID controllers can work within only linear

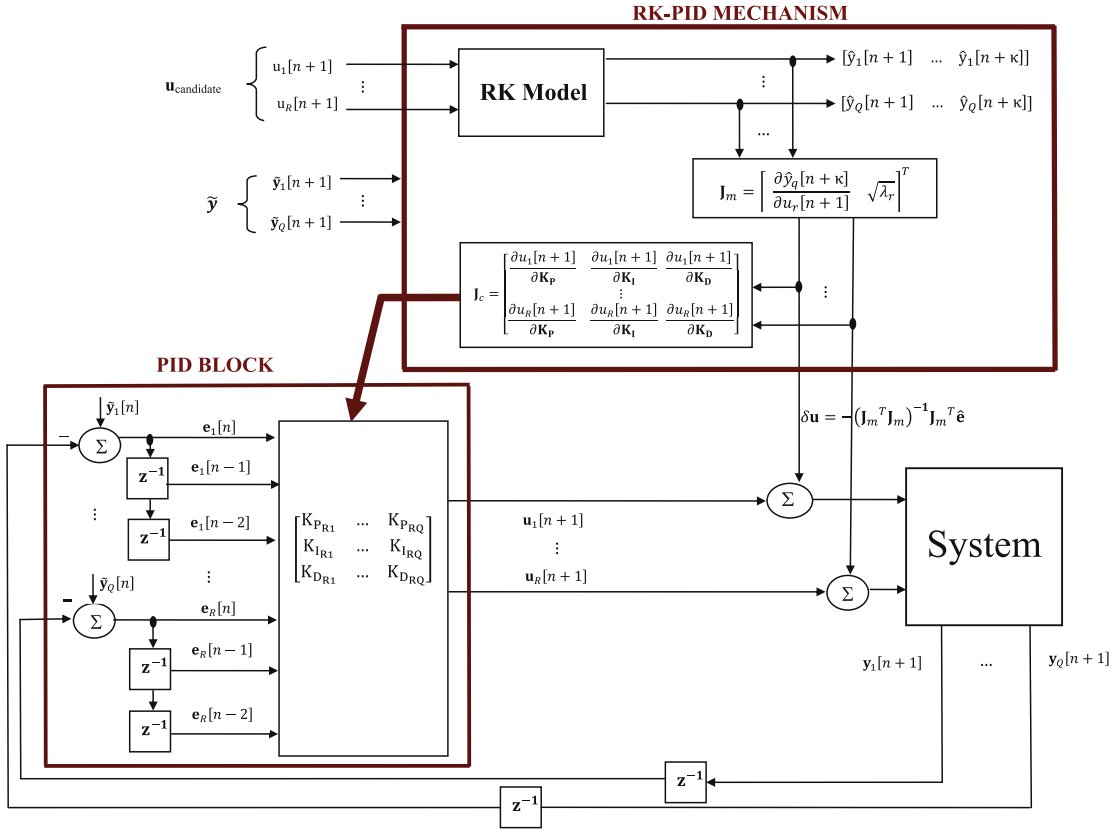

Fig. 1. The structure of RK-PID.

operating range. Structure of the proposed RK model-based PID mechanism is shown in Fig. 1. For multi-step ahead prediction operation, κ defines the prediction horizon. $[\hat{y}_q[n+1], \hat{y}_q[n+2], \ldots, \hat{y}_q[n+\kappa]]$ is the κ-step ahead prediction vector for the q th output of the RK model of the nonlinear system. $\tilde{\mathbf{y}}$ is the reference signal (staircase and/or sinusoidal) the short-term trajectory of which is assumed to be known in advance, $\mathbf{e}[n]$ is the error between the desired and the measured output at the time index n, $\mathbf{u}[n+1]$ is the control signal and $\delta\mathbf{u}[n+1]$ is the correction term. As shown in Fig. 1 the RK-PID controller mechanism consists of two main structures: the RK model of the system and the Jacobian blocks. $\mathbf{J}_m$ is the first Jacobian block which corrects the control signal and $\mathbf{J}_c$ is the second one which tunes the PID controller parameters. The PID controller produces a control signal as

$$\begin{bmatrix} u_1[n+1] \\ \vdots \\ u_R[n+1] \end{bmatrix}_{R\times 1} = \begin{bmatrix} u_1[n] \\ \vdots \\ u_R[n] \end{bmatrix}_{R\times 1} + [\mathbf{K_{PID}}]_{R\times 3Q} \cdot \begin{bmatrix} e_1[n]-e_1[n-1] \\ e_1[n] \\ e_1[n]-2e_1[n-1]+e_1[n-2] \\ \vdots \\ e_Q[n]-e_Q[n-1] \\ e_Q[n] \\ e_Q[n]-2e_Q[n-1]+e_Q[n-2] \end{bmatrix}_{3Q\times 1} \tag{7}$$

where

$$[\mathbf{K_{PID}}]_{R\times 3Q} = \begin{bmatrix} K_{P_{11}} & K_{I_{11}} & K_{D_{11}} & K_{P_{12}} & K_{I_{12}} & K_{D_{12}} & \cdots & K_{P_{1Q}} & K_{I_{1Q}} & K_{D_{1Q}} \\ & & & & \vdots & & & & & \\ K_{P_{R1}} & K_{I_{R1}} & K_{D_{R1}} & K_{P_{R2}} & K_{I_{R2}} & K_{D_{R2}} & \cdots & K_{P_{RQ}} & K_{I_{RQ}} & K_{D_{RQ}} \end{bmatrix}_{R\times 3Q} \tag{8}$$

The terms in (7) can be written in vectorial form as

$$\mathbf{u}[n+1] = \mathbf{u}[n] + \mathbf{K_P}(\mathbf{e}[n]-\mathbf{e}[n-1]) + \mathbf{K_I}\mathbf{e}[n] + \mathbf{K_D}(\mathbf{e}[n]-2\mathbf{e}[n-1]+\mathbf{e}[n-2]), \tag{9}$$

where $\mathbf{K_P}$, $\mathbf{K_I}$ and $\mathbf{K_D}$ are the initially zero PID parameters to be tuned at every iteration by the proposed mechanism. The main issue associated with the RK-PID control is to find optimal values of the PID parameters which are used in the MIMO PID control block also they remain same values during the control phase. When the candidate control signal is applied to the system κ times, the RK model produces the future predictions of the nonlinear system as $[\hat{y}_1[n+1], \ldots, \hat{y}_Q[n+\kappa]]$. Thus, the parameters of the auto-tuning PID control mechanism are updated to minimize F: the sum of the squared κ-step ahead prediction errors given as

$$F(\mathbf{u}[n+1]) = \frac{1}{2}\sum_{p=1}^{\kappa}\sum_{j=1}^{Q}(\tilde{y}_j[n+p]-\hat{y}_j[n+p])^2 + \frac{1}{2}\lambda_r\sum_{r=1}^{R}(u_r[n+1]-u_r[n])^2 \tag{10}$$

where λ_r is the penalty term related to the rth input and the minimization of (10) is accomplished by the Levenberg–Marquardt (LM) algorithm. Finally, the update rule for the PID parameters is given as

$$\begin{bmatrix} \mathbf{K_P} \\ \mathbf{K_I} \\ \mathbf{K_D} \end{bmatrix} \leftarrow \begin{bmatrix} \mathbf{K_P} \\ \mathbf{K_I} \\ \mathbf{K_D} \end{bmatrix} + \Delta\mathbf{K_{PID}} \tag{11}$$

$$\Delta\mathbf{K_{PID}} = -(\mathbf{J}^T\mathbf{J}+\mu\mathbf{I})^{-1}\mathbf{J}^T\hat{\mathbf{e}}. \tag{12}$$

Here, μ provides a good switching between the Steepest Descent and the Gauss Newton directions. During the tuning process, μ is incremented or decremented by a scale at parameter updates. In the update rule, $\mathbf{I}_{3Q\times 3Q}$ is an identity matrix and $\mathbf{J}$ is a

$(Q\kappa+R)\times 3Q$ Jacobian matrix given by

$$\mathbf{J}=\begin{bmatrix} \frac{\partial \hat{e}_1[n+1]}{\partial \mathbf{K_P}} & \frac{\partial \hat{e}_1[n+1]}{\partial \mathbf{K_I}} & \frac{\partial \hat{e}_1[n+1]}{\partial \mathbf{K_D}} \\ \vdots & \vdots & \vdots \\ \frac{\partial \hat{e}_Q[n+\kappa]}{\partial \mathbf{K_P}} & \frac{\partial \hat{e}_Q[n+\kappa]}{\partial \mathbf{K_I}} & \frac{\partial \hat{e}_Q[n+\kappa]}{\partial \mathbf{K_D}} \\ \frac{\partial \sqrt{\lambda_1}\Delta\mathbf{u}[n+1]}{\partial \mathbf{K_P}} & \frac{\partial \sqrt{\lambda_1}\Delta\mathbf{u}[n+1]}{\partial \mathbf{K_I}} & \frac{\partial \sqrt{\lambda_1}\Delta\mathbf{u}[n+1]}{\partial \mathbf{K_D}} \\ \vdots & \vdots & \vdots \\ \frac{\partial \sqrt{\lambda_R}\Delta\mathbf{u}[n+1]}{\partial \mathbf{K_P}} & \frac{\partial \sqrt{\lambda_R}\Delta\mathbf{u}[n+1]}{\partial \mathbf{K_I}} & \frac{\partial \sqrt{\lambda_R}\Delta\mathbf{u}[n+1]}{\partial \mathbf{K_D}} \end{bmatrix} \tag{13}$$

and $\hat{\mathbf{e}}$ is a $(Q\kappa+R)\times R$ prediction error vector as

$$\hat{\mathbf{e}}=\begin{bmatrix} \hat{e}_1[n+1] \\ \vdots \\ \hat{e}_Q[n+\kappa] \\ \sqrt{\lambda_1}\Delta\mathbf{u}[n+1] \\ \vdots \\ \sqrt{\lambda_R}\Delta\mathbf{u}[n+1] \end{bmatrix}=\begin{bmatrix} \tilde{y_1}[n+1]-\hat{y}_1[n+1] \\ \vdots \\ \tilde{y_Q}[n+\kappa]-\hat{y}_Q[n+\kappa] \\ \sqrt{\lambda_1}\Delta\mathbf{u}[n+1] \\ \vdots \\ \sqrt{\lambda_R}\Delta\mathbf{u}[n+1] \end{bmatrix} \tag{14}$$

where $\Delta\mathbf{u}[n+1]=\mathbf{u}[n+1]-\mathbf{u}[n]$. Since the reference signal is constant, $\mathbf{J}$ can be written as follows:

$$\mathbf{J}=-\begin{bmatrix} \frac{\partial \hat{y}_1[n+1]}{\partial \mathbf{K_P}} & \frac{\partial \hat{y}_1[n+1]}{\partial \mathbf{K_I}} & \frac{\partial \hat{y}_1[n+1]}{\partial \mathbf{K_D}} \\ \vdots & \vdots & \vdots \\ \frac{\partial \hat{y}_Q[n+\kappa]}{\partial \mathbf{K_P}} & \frac{\partial \hat{y}_Q[n+\kappa]}{\partial \mathbf{K_I}} & \frac{\partial \hat{y}_Q[n+\kappa]}{\partial \mathbf{K_D}} \\ \frac{\partial \sqrt{\lambda_1}\Delta\mathbf{u}[n+1]}{\partial \mathbf{K_P}} & \frac{\partial \sqrt{\lambda_1}\Delta\mathbf{u}[n+1]}{\partial \mathbf{K_I}} & \frac{\partial \sqrt{\lambda_1}\Delta\mathbf{u}[n+1]}{\partial \mathbf{K_D}} \\ \vdots & \vdots & \vdots \\ \frac{\partial \sqrt{\lambda_R}\Delta\mathbf{u}[n+1]}{\partial \mathbf{K_P}} & \frac{\partial \sqrt{\lambda_R}\Delta\mathbf{u}[n+1]}{\partial \mathbf{K_I}} & \frac{\partial \sqrt{\lambda_R}\Delta\mathbf{u}[n+1]}{\partial \mathbf{K_D}} \end{bmatrix}_{(Q\kappa+R)\times 3Q} \tag{15}$$

The PID parameters which are tuned by (11) and (12) may not be appropriate enough to produce an optimal control signal ($\mathbf{u}[n+1]$) when the reference signals and dynamics of the system change due to modeling errors and external disturbances. In the case that the PID controller is inadequate, a correction term $\delta\mathbf{u}[n+1]$, which is obtained so as to minimize the F, is added to the control action produced by the mechanism. The second-order Taylor approximation is used to minimize the F with respect to $\delta\mathbf{u}[n+1]$ as follows:

$$F(\mathbf{u}[n+1]+\delta\mathbf{u}[n+1])\cong F(\mathbf{u}[n+1])+\frac{\partial F(\mathbf{u}[n+1])}{\partial(\mathbf{u}[n+1])}\delta\mathbf{u}[n+1]+\frac{1}{2}\frac{\partial^2 F(\mathbf{u}[n+1])}{\partial\mathbf{u}^2[n+1]}(\delta\mathbf{u}[n+1])^2. \tag{16}$$

In order to find the term $\delta\mathbf{u}[n+1]$, the approximate objective function in (16) must be derived with respect to $\delta\mathbf{u}[n+1]$ and then equated to zero:

$$\delta\mathbf{u}[n+1]=-\eta\frac{\frac{\partial F}{\partial\mathbf{u}[n+1]}}{\frac{\partial^2 F}{\partial\mathbf{u}^2[n+1]}}, \tag{17}$$

where $0<\eta<1$ is an adjustable parameter in order for the constraints on the input signals, input-slews and output signals to stay within their allowable limits. Instead of calculating the first- and second-order derivatives in (17), their Jacobian approximations can be preferred due to the computational complexity of the second-order derivatives. In this case, by defining a $(Q\kappa+R)\times R$ dimensional $\mathbf{J}_m$ matrix:

$$\mathbf{J}_m=-\begin{bmatrix} \frac{\partial \hat{y}_1[n+1]}{\partial u_1[n+1]} & \frac{\partial \hat{y}_1[n+1]}{\partial u_2[n+1]} & \cdots & \frac{\partial \hat{y}_1[n+1]}{\partial u_R[n+1]} \\ & & \vdots & \\ \frac{\partial \hat{y}_Q[n+\kappa]}{\partial u_1[n+1]} & \frac{\partial \hat{y}_Q[n+\kappa]}{\partial u_2[n+1]} & \cdots & \frac{\partial \hat{y}_Q[n+\kappa]}{\partial u_R[n+1]} \\ \sqrt{\lambda_1} & \sqrt{\lambda_1} & \cdots & \sqrt{\lambda_1} \\ & & \vdots & \\ \sqrt{\lambda_R} & \sqrt{\lambda_R} & \cdots & \sqrt{\lambda_R} \end{bmatrix}. \tag{18}$$

The Gradient vector and the Hessian matrix approximately in (16) and (17) can be written as follows:

$$\frac{\partial F(\mathbf{u}[n+1])}{\partial\mathbf{u}[n+1]}=2\mathbf{J}_m^T\hat{\mathbf{e}} \quad \text{and} \quad \frac{\partial^2 F(\mathbf{u}[n+1])}{\partial\mathbf{u}^2[n+1]}\cong 2\mathbf{J}_m^T\mathbf{J}_m \tag{19}$$

Then, the correction term can be written as

$$\delta\mathbf{u}[n+1]=-\eta\frac{\mathbf{J}_m^T\hat{\mathbf{e}}}{\mathbf{J}_m^T\mathbf{J}_m}. \tag{20}$$

At this point, the question whether as to the matrix $\mathbf{J}_m^T\mathbf{J}_m$ is invertible may be arisen: this will not bring about a problem as long as the controllability condition is hold. Moreover, the constraints on the input signals, input-slews and output signals are taken into consideration by adjusting η to its largest possible value between 0 and 1. As shown in (20) only the first-order derivatives are required. Now, the Jacobian matrix in (15) can be split into two different matrices ($\mathbf{J}_m$ and $\mathbf{J}_c$) by using the chain rule. Here $\mathbf{J}_c$ is a $R\times 3Q$ matrix of partial derivatives of $\mathbf{u}[n+1]$ with respect to the

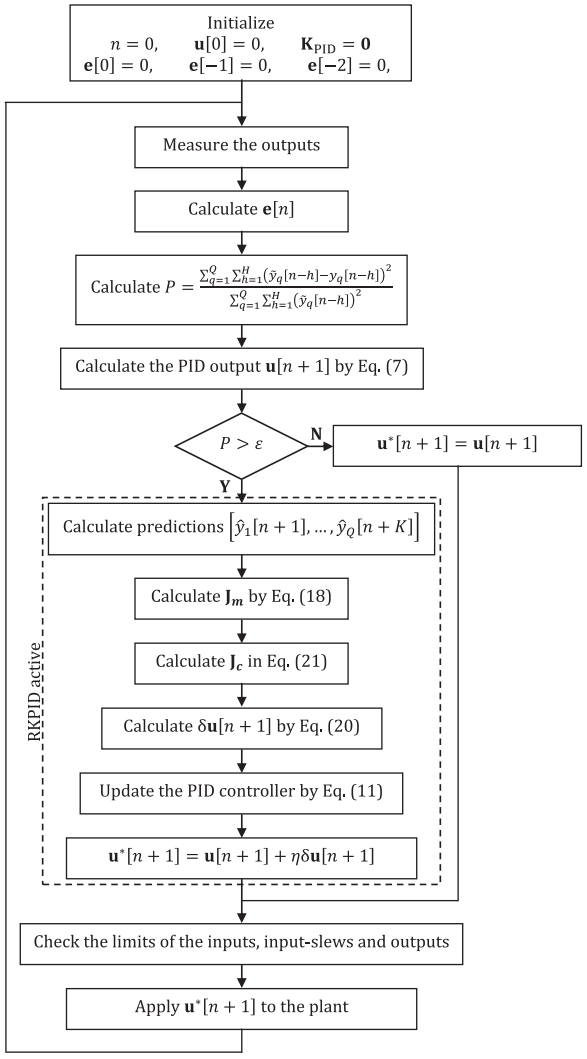

Fig. 2. The flowchart of the proposed RK-PID controller.

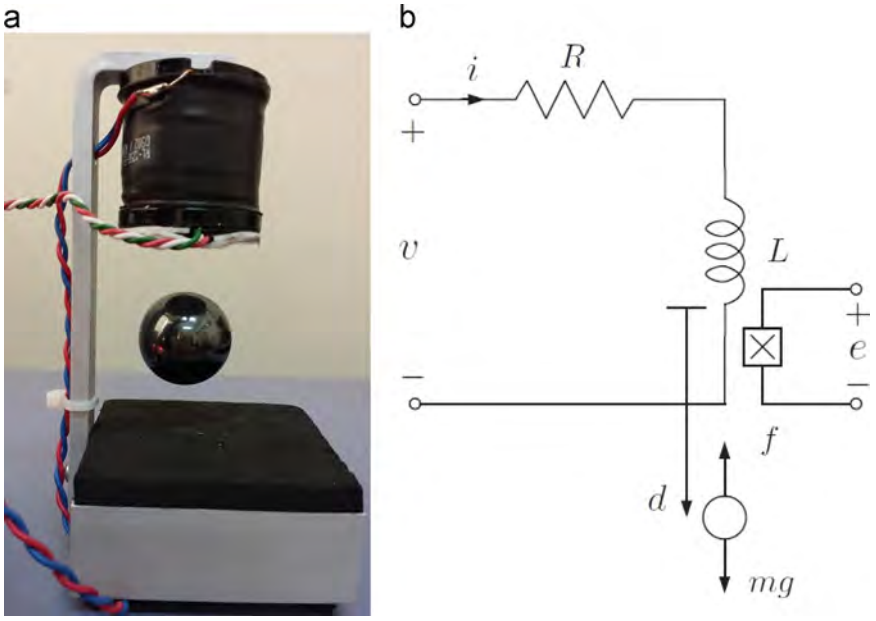

Fig. 3. Magnetic levitation control system and schematic structure. (a) Magnetic levitation control system and (b) schematic structure of the MagLev.

Table 1
The parameters of magnetic levitation system.

Parameter description	Value
R: resistance of the coil	1.71 (Ω)
L: inductance of the coil	15.1×10^{-3} (H)
m: mass of the levitating magnet	41.3×10^{-3} (kg)
k: electromagnet force constant	3.1×10^{-6} (kg m^5/s^2/ A)
α: constant that depends on the hall-effect sensor	2.48 (V)
β: constant that depends on the hall-effect sensor	4.25×10^{-4} (V m^2)
γ: constant that depends on the hall-effect sensor	0.31×10^{-4} (V/A)
g:gravitation coefficient	9.81 (m/s^2)

PID parameters:

$$\mathbf{J}=-\begin{bmatrix} \frac{\partial\hat{y}_1[n+1]}{\partial u_1[n+1]} & \frac{\partial\hat{y}_1[n+1]}{\partial u_2[n+1]} & \cdots & \frac{\partial\hat{y}_1[n+1]}{\partial u_R[n+1]} \\ \vdots & & & \\ \frac{\partial\hat{y}_Q[n+\kappa]}{\partial u_1[n+1]} & \frac{\partial\hat{y}_Q[n+\kappa]}{\partial u_2[n+1]} & \cdots & \frac{\partial\hat{y}_Q[n+\kappa]}{\partial u_R[n+1]} \\ \sqrt{\lambda_1} & \sqrt{\lambda_1} & \cdots & \sqrt{\lambda_1} \\ & \vdots & & \\ \sqrt{\lambda_R} & \sqrt{\lambda_R} & \cdots & \sqrt{\lambda_R} \end{bmatrix}\begin{bmatrix} \frac{\partial u_1[n+1]}{\partial K_{P_{11}}} & \cdots & \frac{\partial u_1[n+1]}{\partial K_{D_{RQ}}} \\ & \vdots & \\ \frac{\partial u_R[n+1]}{\partial K_{P_{11}}} & \cdots & \frac{\partial u_R[n+1]}{\partial K_{D_{RQ}}} \end{bmatrix} \tag{21}$$

The κ-step ahead future predictions of the plant outputs can be calculated by using the RK model of the system if Eq. (5) is employed in an iterative way. In the iterations, the candidate control vector $\mathbf{u}[n+1]$ is assumed to remain unchanged during the prediction interval ($[t+T_s\ t+\kappa T_s]$). Hence, a series of future predictions is obtained for each output as $[\hat{y}_1[n+1],\ldots,\hat{y}_Q[n+\kappa]]$. Now, the problem of calculation of the derivatives in $\mathbf{J}_m$ is turned out to that of the terms $\partial\hat{y}_1[n+1]/\partial\mathbf{u}[n+1],\ldots,\partial\hat{y}_Q[n+\kappa]/\partial\mathbf{u}[n+1]$, which can be handled using chain rule as follows ($p=1,\ldots,\kappa$):

$$\frac{\partial\hat{y}_Q[n+\kappa]}{\partial\mathbf{u}[n+1]}=\frac{\partial^T\mathbf{g}}{\partial\mathbf{x}}\bigg|_{\mathbf{x}=\hat{\mathbf{x}}[n+p]}\frac{\partial\hat{\mathbf{x}}[n+p]}{\partial\mathbf{u}[n+1]}. \tag{22}$$

According to (22), the term $\partial\hat{\mathbf{x}}[n+p]/\partial\mathbf{u}[n+1]$ is calculated by using the RK model of the system. Then, the partial derivatives are obtained by

$$\frac{\partial\hat{\mathbf{x}}[n+p]}{\partial\mathbf{u}[n+1]}=\frac{\partial\hat{\mathbf{f}}}{\partial\mathbf{x}}\bigg|_{\substack{\mathbf{x}=\hat{\mathbf{x}}[n+p-1]\\ \mathbf{u}[n+1]=\mathbf{u}[n+1]}}\frac{\partial\hat{\mathbf{x}}[n+p-1]}{\partial\mathbf{u}[n+1]}+\frac{\partial\hat{\mathbf{f}}}{\partial\mathbf{u}[n+1]}\bigg|_{\substack{\mathbf{x}=\hat{\mathbf{x}}[n+p-1]\\ \mathbf{u}[n+1]=\mathbf{u}[n+1]}} \tag{23}$$

where

$$\frac{\partial\hat{\mathbf{f}}}{\partial\mathbf{x}[n]}=\frac{\partial\mathbf{x}_i[n]}{\partial\mathbf{x}[n]}+\frac{1}{6}\left(\frac{\partial\mathbf{k}_1}{\partial\mathbf{x}[n]}+2\frac{\partial\mathbf{k}_2}{\partial\mathbf{x}[n]}+2\frac{\partial\mathbf{k}_3}{\partial\mathbf{x}[n]}+\frac{\partial\mathbf{k}_4}{\partial\mathbf{x}[n]}\right), \tag{24}$$

and

$$\frac{\partial\hat{\mathbf{f}}}{\partial\mathbf{u}[n+1]}=\frac{1}{6}\left(\frac{\partial\mathbf{k}_1}{\partial\mathbf{u}[n+1]}+2\frac{\partial\mathbf{k}_2}{\partial\mathbf{u}[n+1]}+2\frac{\partial\mathbf{k}_3}{\partial\mathbf{u}[n+1]}+\frac{\partial\mathbf{k}_4}{\partial\mathbf{u}[n+1]}\right), \tag{25}$$

where the partial derivatives with respect to states in (24) are obtained as follows:

$$\frac{\partial\mathbf{k}_1}{\partial\mathbf{x}[n]}=T_s\frac{\partial\mathbf{f}}{\partial\mathbf{x}[n]}\bigg|_{\substack{\mathbf{x}[n]=\mathbf{x}[n]\\ \mathbf{u}[n]=\mathbf{u}[n]}}, \tag{26}$$

$$\frac{\partial\mathbf{k}_2}{\partial\mathbf{x}[n]}=T_s\left(\frac{\partial\mathbf{f}}{\partial\mathbf{x}[n]}\bigg|_{\substack{\mathbf{x}[n]=\mathbf{x}[n]+0.5\mathbf{k}_1\\ \mathbf{u}[n]=\mathbf{u}[n]}}\left(\mathbf{I}+0.5\frac{\partial\mathbf{k}_1}{\partial\mathbf{x}[n]}\right)\right), \tag{27}$$

$$\frac{\partial\mathbf{k}_3}{\partial\mathbf{x}[n]}=T_s\left(\frac{\partial\mathbf{f}}{\partial\mathbf{x}[n]}\bigg|_{\substack{\mathbf{x}[n]=\mathbf{x}[n]+0.5\mathbf{k}_2\\ \mathbf{u}[n]=\mathbf{u}[n]}}\left(\mathbf{I}+0.5\frac{\partial\mathbf{k}_2}{\partial\mathbf{x}[n]}\right)\right), \tag{28}$$

$$\frac{\partial\mathbf{k}_4}{\partial\mathbf{x}[n]}=T_s\left(\frac{\partial\mathbf{f}}{\partial\mathbf{x}[n]}\bigg|_{\substack{\mathbf{x}[n]=\mathbf{x}[n]+\mathbf{k}_3\\ \mathbf{u}[n]=\mathbf{u}[n]}}\left(\mathbf{I}+\frac{\partial\mathbf{k}_3}{\partial\mathbf{x}[n]}\right)\right), \tag{29}$$

and the partial derivatives with respect to control signals in (25) are obtained as follows:

$$\frac{\partial\mathbf{k}_1}{\partial\mathbf{u}[n]}=T_s\frac{\partial\mathbf{f}}{\partial\mathbf{u}[n]}\bigg|_{\substack{\mathbf{x}[n]=\mathbf{x}[n]\\ \mathbf{u}[n]=\mathbf{u}[n]}}, \tag{30}$$

$$\frac{\partial\mathbf{k}_2}{\partial\mathbf{u}[n]}=T_s\left(0.5\frac{\partial\mathbf{f}}{\partial\mathbf{x}}\bigg|_{\substack{\mathbf{x}[n]=\mathbf{x}[n]+0.5\mathbf{k}_1\\ \mathbf{u}[n]=\mathbf{u}[n]}}\frac{\partial\mathbf{k}_1}{\partial\mathbf{u}[n]}+\frac{\partial\mathbf{f}}{\partial\mathbf{u}[n]}\bigg|_{\substack{\mathbf{x}[n]=\mathbf{x}[n]+0.5\mathbf{k}_1\\ \mathbf{u}[n]=\mathbf{u}[n]}}\right), \tag{31}$$

$$\frac{\partial\mathbf{k}_3}{\partial\mathbf{u}[n]}=T_s\left(0.5\frac{\partial\mathbf{f}}{\partial\mathbf{x}}\bigg|_{\substack{\mathbf{x}[n]=\mathbf{x}[n]+0.5\mathbf{k}_2\\ \mathbf{u}[n]=\mathbf{u}[n]}}\frac{\partial\mathbf{k}_2}{\partial\mathbf{u}[n]}+\frac{\partial\mathbf{f}}{\partial\mathbf{u}[n]}\bigg|_{\substack{\mathbf{x}[n]=\mathbf{x}[n]+0.5\mathbf{k}_2\\ \mathbf{u}[n]=\mathbf{u}[n]}}\right), \tag{32}$$

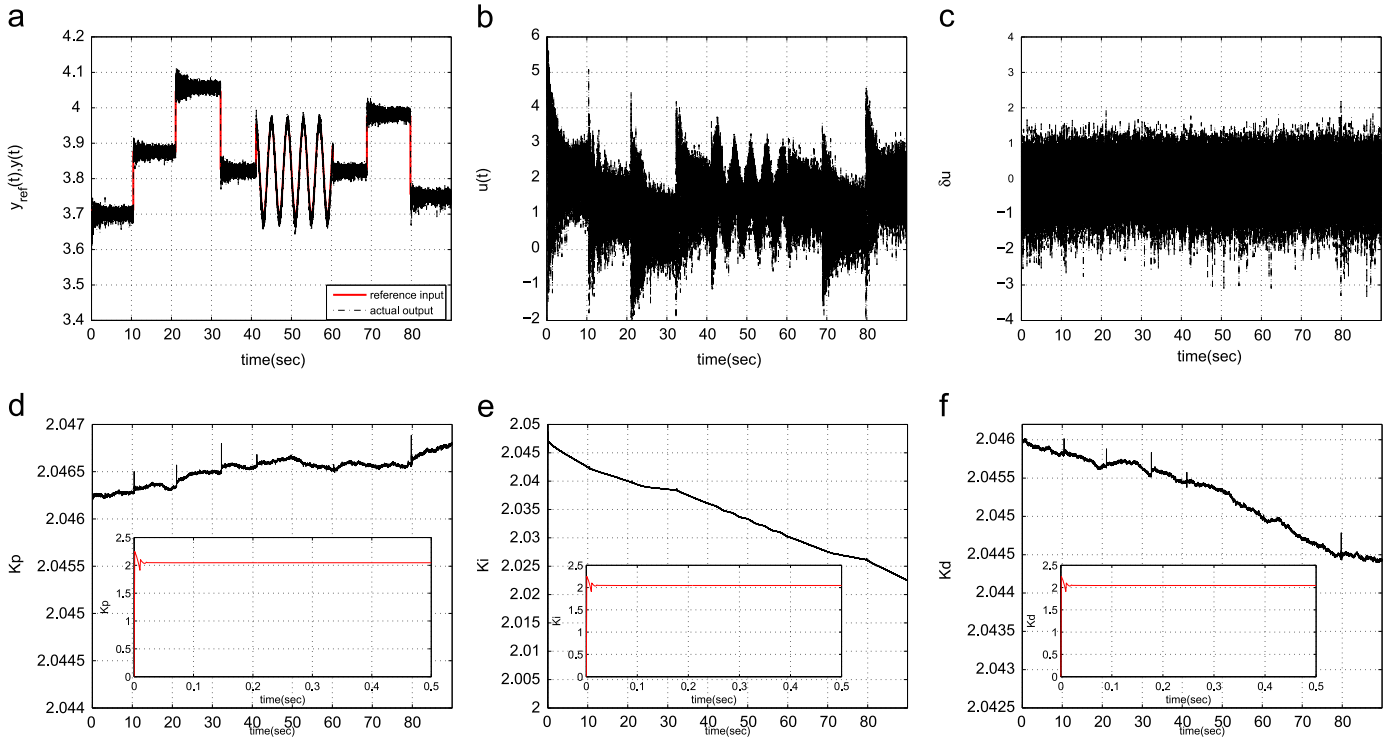

Fig. 4. Real-time experimental results of the MagLev for RK-PID. (a) Voltage value of the output sensor, (b) control voltage, (c) correction term of the MagLev, (d) K_P, (e) K_I, and (f) K_D.

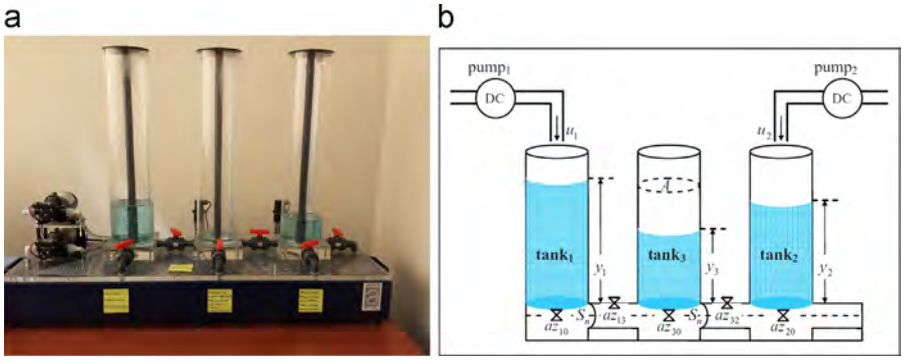

Fig. 5. Three-tank liquid-level control system and schematic structure. (a) Three-tank liquid-level control system and (b) schematic structure of the liquid-level system.

$$\frac{\partial \mathbf{k}_4}{\partial \mathbf{u}[n]} = T_s \left(\frac{\partial \mathbf{f}}{\partial \mathbf{x}}\bigg|_{\substack{\mathbf{x}[n]=\mathbf{x}[n]+\mathbf{k}_3 \\ \mathbf{u}[n]=\mathbf{u}[n]}} \frac{\partial \mathbf{k}_3}{\partial \mathbf{u}[n]} + \frac{\partial \mathbf{f}}{\partial \mathbf{u}[n]}\bigg|_{\substack{\mathbf{x}[n]=\mathbf{x}[n]+\mathbf{k}_3 \\ \mathbf{u}[n]=\mathbf{u}[n]}} \right). \tag{33}$$

Finally, for better understanding, a flowchart describing the algorithm is given in Fig. 2.

4. Experimental results

In this section, the proposed model predictive RK-PID mechanism is tested on two nonlinear real-time experimental systems. These systems are nonlinear the magnetic levitation system [33] and the three-tank liquid-level system [34]. The aim of the designed mechanism is to adjust the PID controller parameters to be used for real-time control.

4.1. Magnetic levitation system (MagLev)

The magnetic levitation experimental set-up is originally unstable, extremely challenging to control robustly and it is highly nonlinear SISO process as shown in Fig. 3. MagLev controls the magnetic field generated by an electromagnet to levitate a small permanent magnet in mid-air. The vertical position of the levitating magnet is measured using a linear hall-effect sensor and the current in the electromagnet is actively controlled to achieve stable levitation. This system is fully compatible with the HILINK

Table 2
The parameters of three-tank liquid-level control system.

Parameter description	Value
$x_i(t)$: liquid level of tank$_i$	ith output (m)
$u_i(t)$: supplying flow rate of pump$_i$	ith input (m^3/s)
az_{13}: outflow coefficient between tank$_1$ and tank$_3$	0.0280
az_{32}: outflow coefficient between tank$_3$ and tank$_2$	0.2569
az_{10}: outflow coefficient between tank$_1$ and tank$_0$	0.5510
az_{20}: outflow coefficient between tank$_2$ and tank$_0$	0.2459
az_{30}: outflow coefficient between tank$_3$ and tank$_0$	0.5457
A: section of cylinders	0.0154 (m^2)
S_n: section of connection pipe n	5×10^{-5} (m^2)
g: gravitation coefficient	9.81 (m/s^2)

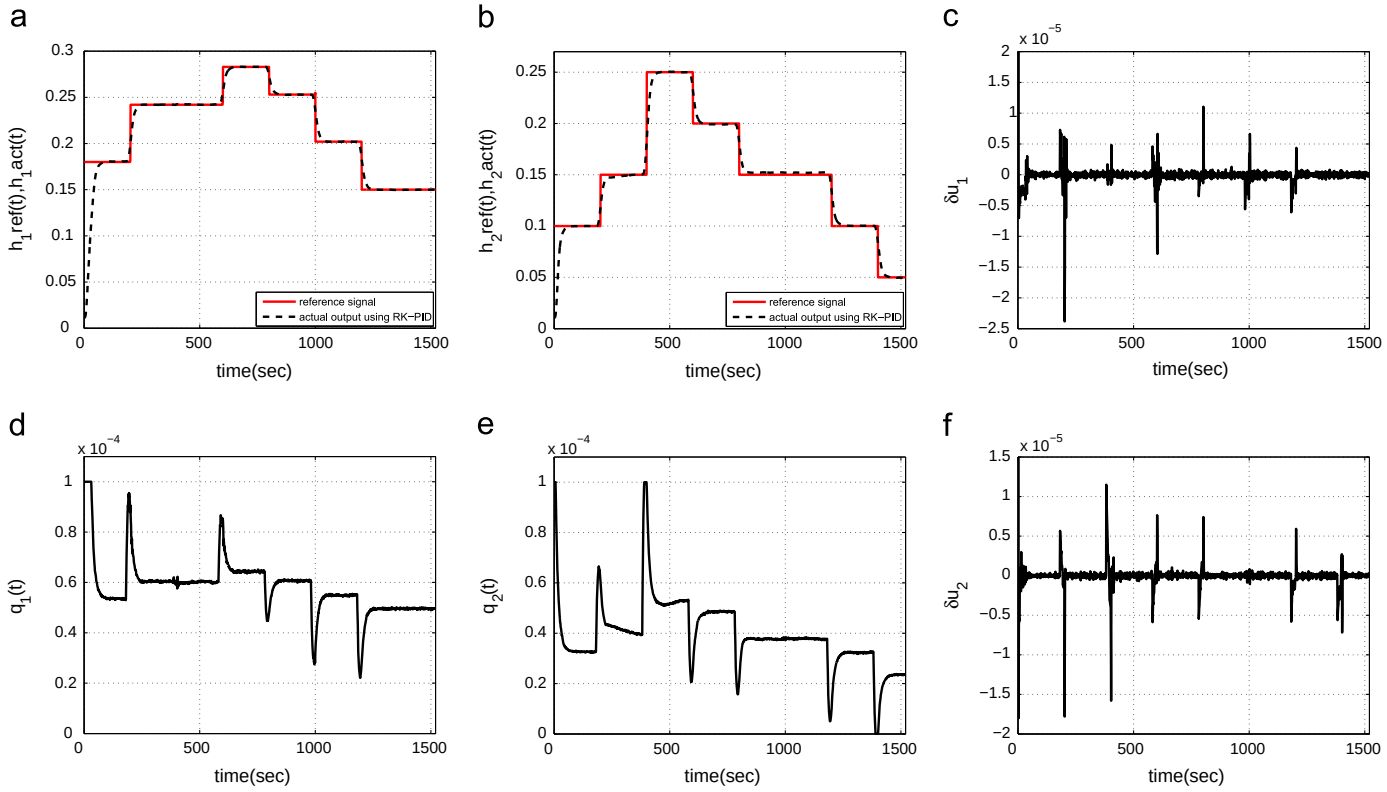

Fig. 6. Real-time experimental results of the liquid-level system for RK-PID (without measurement noise). (a) Liquid-level of tank$_1$, (b) liquid-level of tank$_2$, (c) correction term of tank$_1$, (d) control signal of pump$_1$, (e) control signal of pump$_2$, and (f) correction term of tank$_2$.

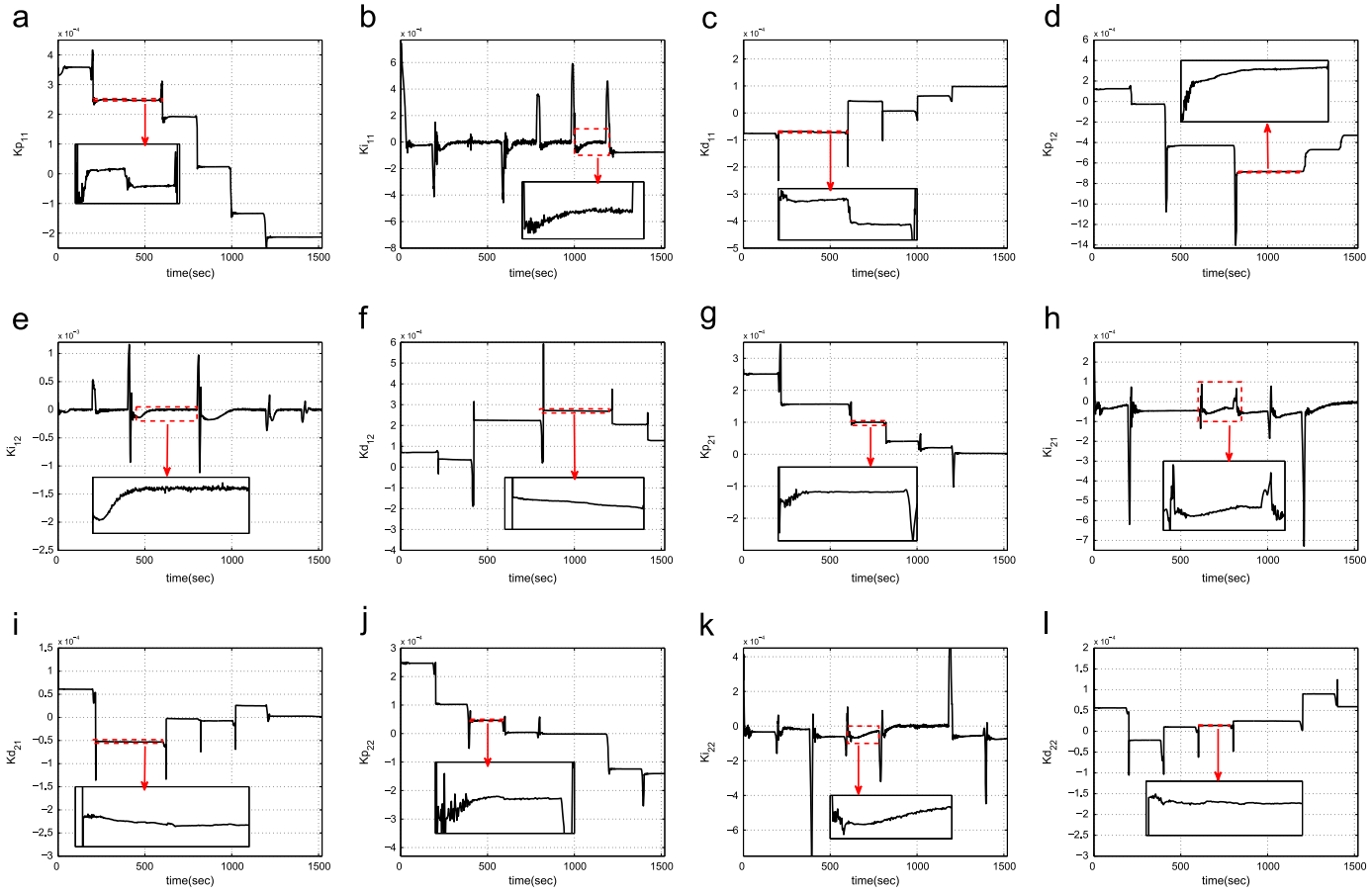

Fig. 7. The PID parameters of the RK-PID controller. (a) $K_{P_{11}}$, (b) $K_{I_{11}}$, (c) $K_{D_{11}}$, (d) $K_{P_{12}}$, (e) $K_{I_{12}}$, (f) $K_{D_{12}}$, (g) $K_{P_{21}}$, (h) $K_{I_{21}}$, (i) $K_{D_{21}}$, (j) $K_{P_{22}}$, (k) $K_{I_{22}}$, and (l) $K_{D_{22}}$

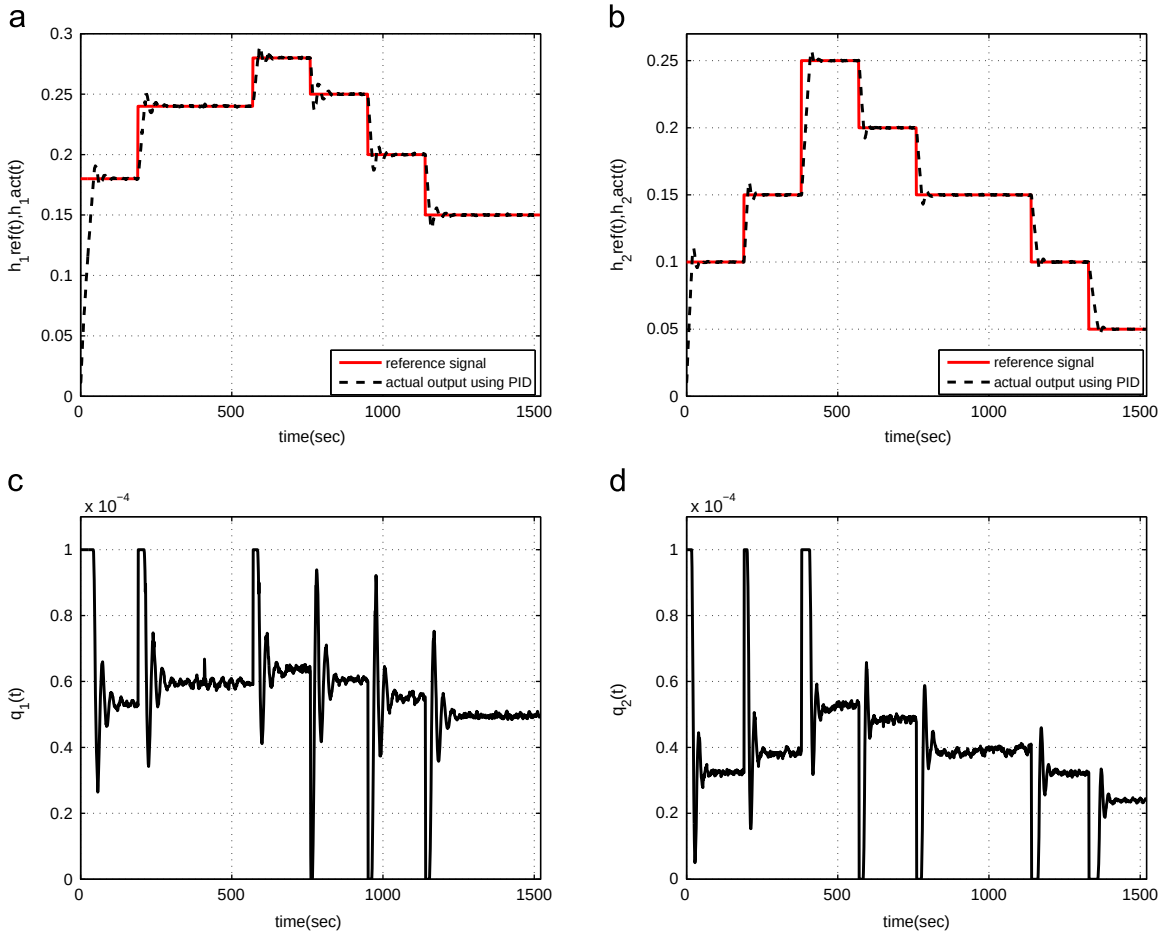

Fig. 8. Real-time experimental results of the liquid-level system for PID (without measurement noise). (a) Liquid-level of tank$_1$, (b) liquid-level of tank$_2$, (c) control signal of pump$_1$, and (d) control signal of pump$_2$.

(hardware-in-the-loop real-time control platform for Matlab/Simulink) and RAPCON (real-time rapid control prototyping platform for Matlab/Simulink) platforms. Mathematical model of this system [33] is given as

$$\dot{x}_1(t) = x_2(t),$$
$$\dot{x}_2(t) = -\frac{k}{m}\frac{x_3(t)}{x_1^3(t)} + g,$$
$$\dot{x}_3(t) = -\frac{R}{L}x_3(t) + \frac{1}{L}u(t). \tag{34}$$

The voltage across the hall-effect sensor induced by the levitating magnet and the coil can be closely approximated as

$$e(t) = \beta\frac{1}{x_1^2(t)} + \gamma x_3(t) + \alpha, \tag{35}$$

where d is the vertical position of the levitating magnet measured from the bottom of the electromagnet, i is the current through the electromagnet, v is the voltage across the electromagnet, $y = e$ (measured output) and $u = v$ be the control input. $x = [x_1\ x_2\ x_3] = [d\ \dot{d}\ i]$ is the state vector of the system. The parameters of the magnetic levitation system are given in Table 1. The purpose in this experiment is to control the vertical position of the levitating magnet by manipulating the control signal. The limits of the control signal are $u_{min} = -7$ V and $u_{max} = 7$ V, the limits of the output signal are $y_{min} = 0$ V and $y_{max} = 5$ V and the sampling period is used as $T_s = 0.001$ s. For a satisfactory control performance, the design parameters of RK-PID are set to optimum values that have been found by using grid-search of a reasonable interval as follows: (i) $\kappa = 7$, (ii) $\lambda = 0.06$, (iii) $\mu = 100$. Fig. 4 shows the real-time results for RK-PID structure and the PID parameters related to control action. It can be observed from the experimental results that the output of the MagLev system tracks the given mixed (staircase and sinusoidal) reference trajectory and that the control signal is adjusted for the best control action within the limits of the input signal. The correction term, which changes adaptively as in the Fig. 4(c), indicates the effectiveness of the RK-PID controller. A relatively small correction term implies that the tuned PID parameters are very close to their optimal values. Observations of the relatively more fluctuations than those for the liquid-level system can be attributable to the fact that MagLev is highly nonlinear and unstable system. The PID parameters related to the position of the levitating magnet have been converged to their optimal values when the reference signals are changed.

4.2. Three-tank liquid-level system

The three-tank liquid-level system is a nonlinear MIMO real-time experimental system as shown in Fig. 5. This system consists of three interconnected cylindrical tanks, two pumps, six valves, water reservoir in the bottom. The pumps pump water from the bottom to the top of the left and right tanks. Valve positions are controlled and measured by electrical signals which allow precise positioning. Pumps are controlled by analogue signals in range from -10 V to 10 V. Heights of water levels are measured by pressure sensors [34]. The dynamics of the system can be

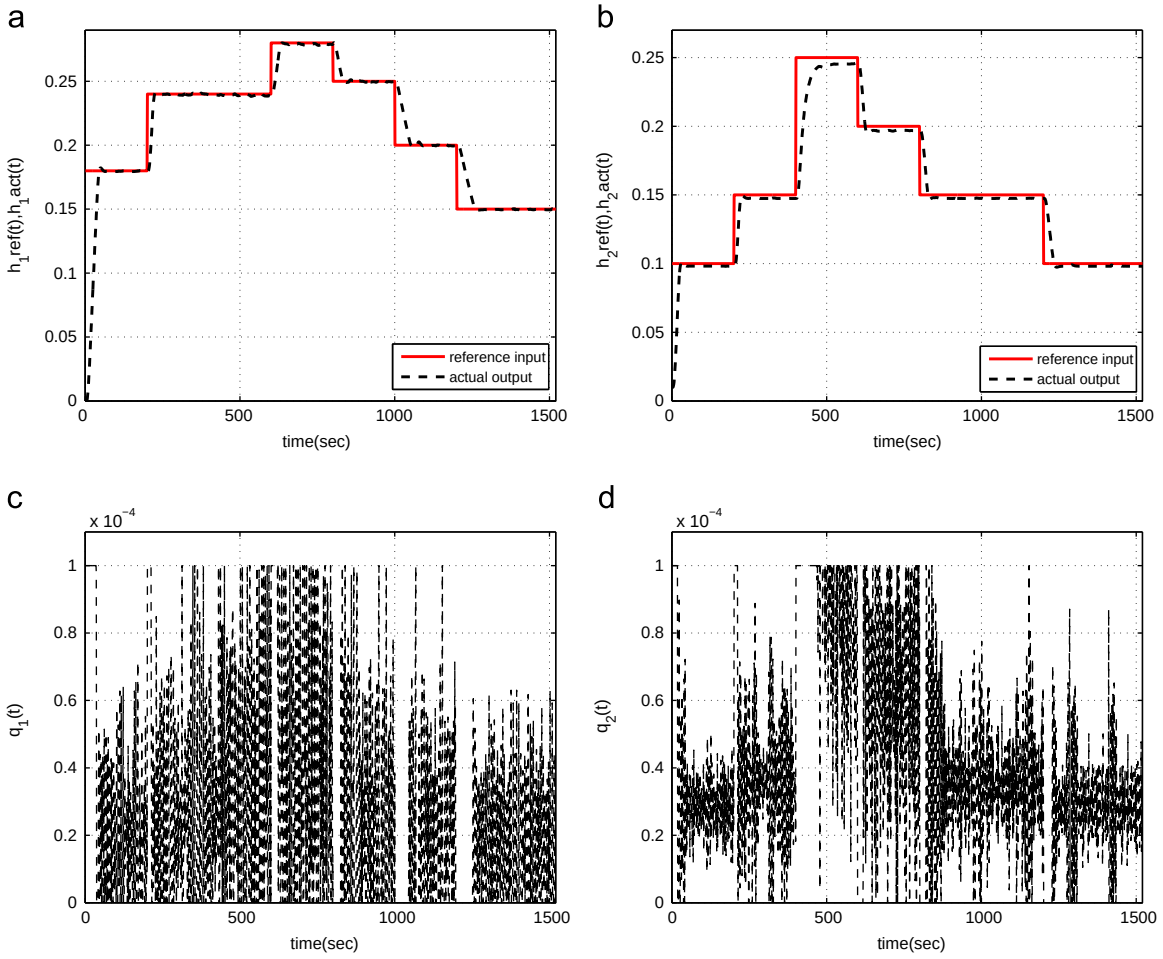

Fig. 9. Real-time experimental results of the liquid-level system for SMC (without measurement noise). (a) Liquid-level of tank_1, (b) liquid-level of tank_2, (c) control signal of pump_1, and (d) control signal of pump_2.

expressed by a set of differential equations as

$$\dot{x}_1(t) = \frac{1}{A}[u_1(t) - Q_{13}(t) - Q_{10}(t)],$$
$$\dot{x}_2(t) = \frac{1}{A}[u_2(t) + Q_{32}(t) - Q_{20}(t)],$$
$$\dot{x}_3(t) = \frac{1}{A}[Q_{13}(t) - Q_{32}(t) - Q_{30}(t)], \tag{36}$$

where

$$Q_{13}(t) = az_{13}S_n \operatorname{sgn}(x_1(t) - x_3(t))\sqrt{2g|x_1(t) - x_3(t)|},$$
$$Q_{32}(t) = az_{32}S_n \operatorname{sgn}(x_3(t) - x_2(t))\sqrt{2g|x_3(t) - x_2(t)|},$$
$$Q_{10}(t) = az_{10}\, S_n\sqrt{2gx_1(t)},$$
$$Q_{20}(t) = az_{20}\, S_n\sqrt{2gx_2(t)},$$
$$Q_{30}(t) = az_{30}\, S_n\sqrt{2gx_3(t)}, \tag{37}$$

where u_i is the supplying flow rate of pump_i as the ith input and x_i is the liquid-level of tank_i as the ith output of the controlled plant. The numerical values of the parameters for the liquid-level system are given in Table 2, which are determined approximately by visual analysis; that is, the outflow parameters correspond to the positions of the valves between the tanks and the reservoir, and thus, it is not possible to find the exact values of the parameters accurately. The purpose in this experiment is to control the liquid-level of tank_1 and tank_2. The limits of the control signals are $u_{1\min} = u_{2\min} = 0\ \text{m}^3/\text{s}$ and $u_{1\max} = u_{2\max} = 0.0001\ \text{m}^3/\text{s}$, the limits of the output signals are $y_{1\min} = y_{2\min} = 0\ \text{m}$ and $y_{1\max} = y_{2\max} = 0.6\ \text{m}$ and the sampling period is used as $T_s = 1.0\ \text{s}$. For a satisfactory control performance, the design parameters of RK-PID are determined as optimum values through grid-search of a reasonable interval as follows: (i) $\kappa = 20$, (ii) $\lambda = 0.01$, (iii) $\mu = 10$. Fig. 6 shows the real-time application results obtained using the RK-PID structure. Based on these results, it is observed that the outputs of the liquid-level system can accurately track the given reference trajectories and that the input signals have been manipulated to achieve a satisfactory control performance at every sampling time. Fig. 6(c) and (f) illustrates the correction terms produced by the mechanism, where the spikes are observed at the time instants when the reference trajectories are changed abruptly. Except for the times when the spikes occur, the correction terms tend to zero, which indicates the effectiveness of the mechanism. When δu_{n+1} is close to zero it means that the control performance of PID is acceptable. The PID parameters related to coupled tanks are given in the Fig. 7 where the PID parameters have been converged to their optimal values when the reference signals are changed.

4.3. Comparisons to other methods

In order to assess the efficiency of the RK-PID, the same experiments have been repeated for the conventional PID controller, the parameters of which have been optimized by the Big-Bang Big-Crunch algorithm as given in [35], the standard nonlinear MPC [36], RK-MPC [29] and also standard SMC [37,38]. As can be seen from Fig. 8, controlled by the standard PID, the outputs of the three-tank system can reach the reference values as fast as in the

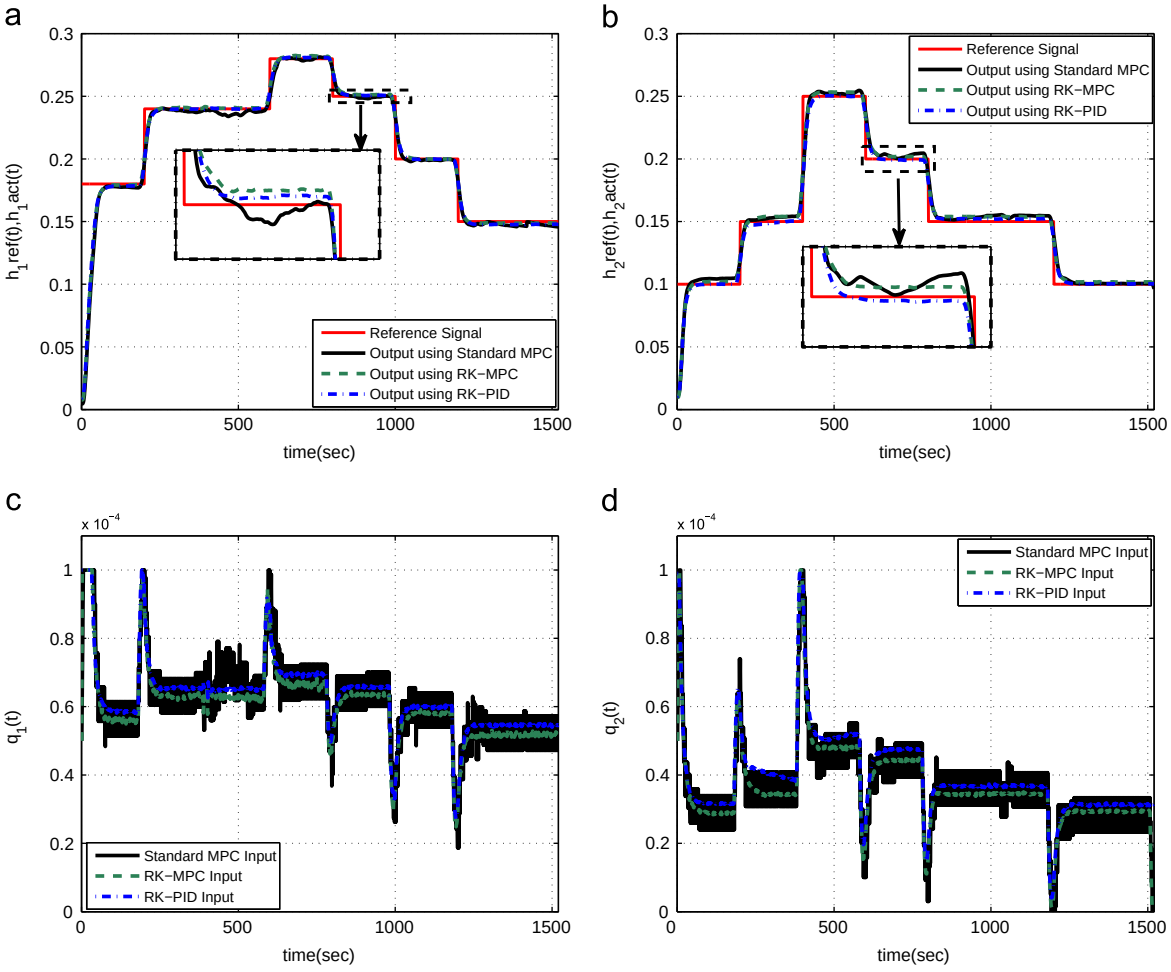

Fig. 10. Comparisons to standard MPC, RK-MPC and RK-PID (without measurement noise). (a) Liquid-level of $tank_1$, (b) liquid-level of $tank_2$, (c) control signal of $pump_1$, and (d) control signal of $pump_2$.

Table 3
Comparisons to other methods (in RMSE).

Without measurement noise	PID	NMPC	SMC	RK – MPC	RK – PID
$tank_1$	0.0339	0.0125	0.0121	0.0119	0.0113
$tank_2$	0.0204	0.0114	0.0118	0.00957	0.00923
With shot noise	PID	NMPC	SMC	RK – MPC	RK – PID
$tank_1$	0.0474	0.0235	0.0225	0.0217	0.0203
$tank_2$	0.0286	0.0137	0.0128	0.0124	0.0111
With measurement noise	PID	NMPC	SMC	RK – MPC	RK – PID
$tank_1$	0.0672	0.0265	0.0261	0.0232	0.0234
$tank_2$	0.0540	0.0172	0.0256	0.0148	0.0151
With measurement noise	PID	NMPC	SMC	RK – MPC	RK – PID
MagLev	–	0.0202	0.2017	0.1564	0.1325

RK-PID case. However, the standard PID causes an approximately 10 percent overshoot and some oscillations leading to longer settling time. The reason why the proposed RK-PID method performs better than the standard PID with respect to the transient-time specifications is that RK-PID works in a predictive manner and gets benefit from the short-term knowledge of the reference signal. Fig. 9 shows the real-time experimental results of the liquid-level system for SMC without measurement noise. The fact that SMC is an easy-to-implement method and it is considerably robust against model uncertainties has been observed in the experiments. Furthermore, Fig. 10 illustrates the comparisons of RK-PID to the standard MPC and RK-MPC, where it is observed that RK-PID and RK-MPC yield similar performances that are better than that of the standard MPC. Overall performances of all controllers have been given in Table 3 numerically. To compare the robustness of the controllers against shot noises incorporated with the control input and the reference signal, some bounded shot noises are added to the input and the reference as seen in Fig. 11. The results show that RK-PID is more robust against external unknown disturbances than the standard SMC and conventional PID since the former yields better RMSE performance (Table 3) and gives less oscillatory response than the latter does. Moreover, in order to compare the robustness of the controllers against measurement noises, the experiments have been repeated in the pick hours when the electromagnetic interferences on the measurement devices get their highest values. The results are illustrated in Figs. 12 and 13. As can be seen from the figures and Table 3, the proposed mechanism provides better results than the standard SMC and classical PID controller. In the noiseless case, SMC performs an intermediate control compared to others, while its performance degrades when the shot noise and measurement noise are incorporated. In both noisy and noiseless cases, chattering problem at the SMC control signals have been observed, which is the major disadvantage of the SMC-type methods even saturation function has been used.

On the other hand, the same comparisons have been attempted to be performed for the MagLev system. However, the standard PID controller is not able to control the MagLev system in its whole working space. In other words, when the magnetic sphere is on the ground, to steer the sphere from the ground to a desired point

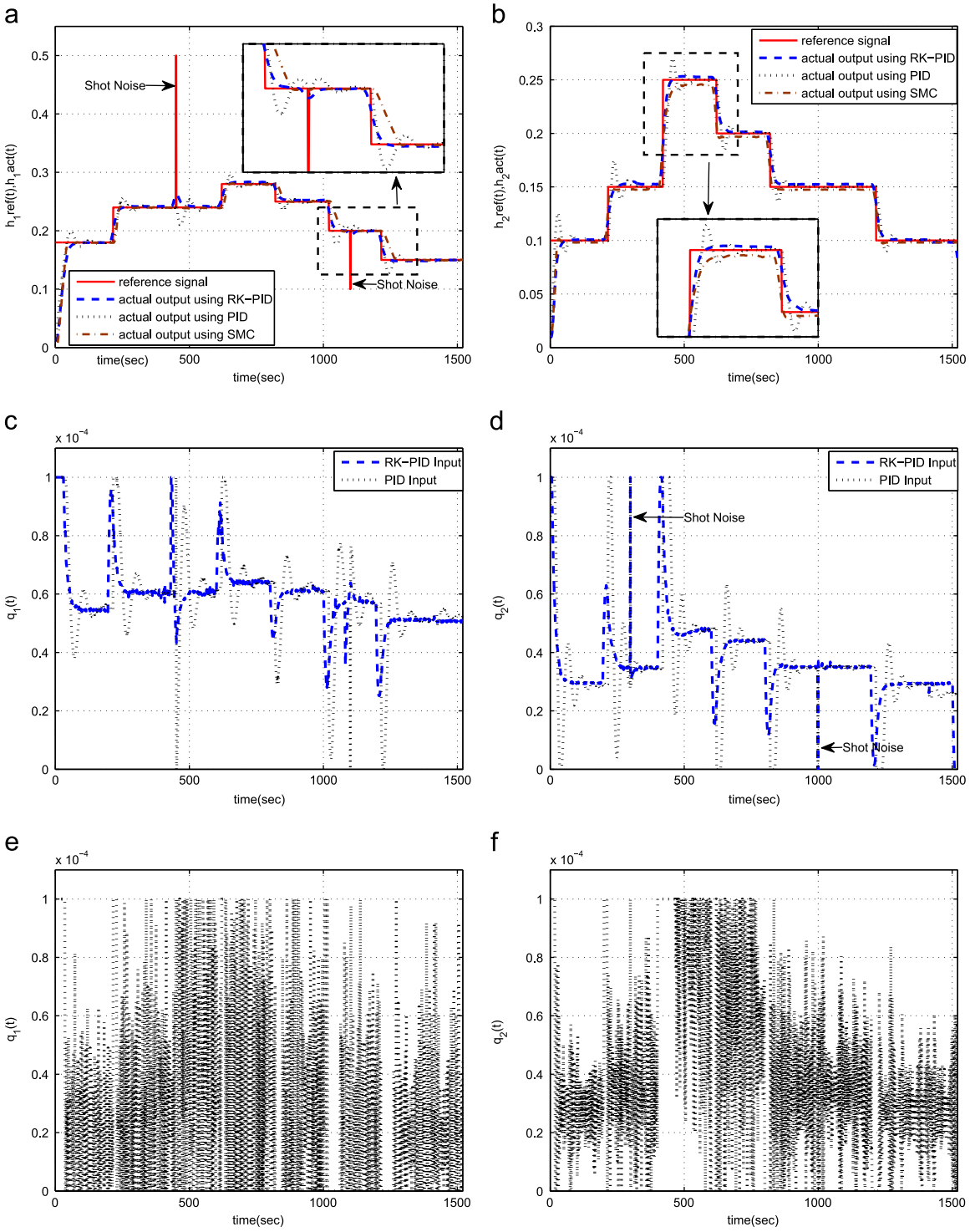

Fig. 11. Real-time experimental results of the liquid-level system (with shot noise). (a) Liquid-level of $tank_1$, (b) liquid-level of $tank_2$, (c) control signal of $pump_1$, (d) control signal of $pump_2$, (e) control signal of $pump_1$ for SMC and (f) control signal of $pump_2$ for SMC.

in the air is a nonlinear control problem which cannot be achieved by the standard PID controller that can work only in local linear region. This can be regarded as another superiority of RK-PID to the standard PID. Therefore, comparisons to the standard PID have been limited for only the three-tank system. As far as the other MPC methods and standard SMC are concerned, the proposed RK-PID has been compared to them for only the case where there are only measurement noises since the additive shot noise pushes the ball either to the ground or ceil and makes the control extremely difficult. As can be seen from Table 3, where the numerical results have been tabulated, the proposed mechanism provides better performance than other methods. In addition to the control performance, all controllers have been compared with respect to computation time which is defined to be the duration between the measurements and the calculation of the control signals. As can be seen from the results, tabulated in Table 4, the conventional PID is

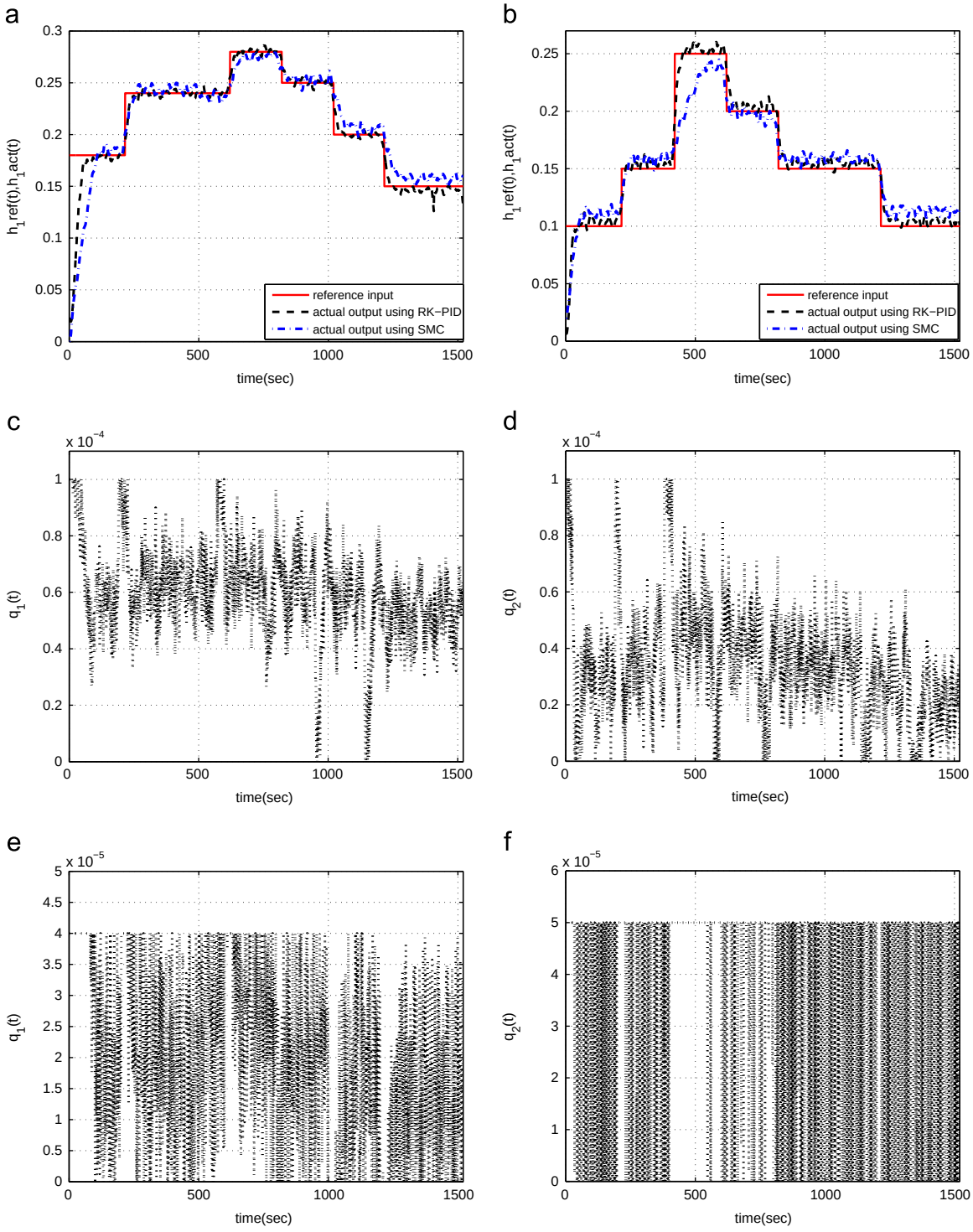

Fig. 12. Real-time experimental results of the liquid-level system (with measurement noise). (a) Liquid-level of $tank_1$, (b) liquid-level of $tank_2$, (c) control signal of $pump_1$ for RK-PID, (d) control signal of $pump_2$ for RK-PID, (e) control signal of $pump_1$ for SMC and (f) control signal of $pump_2$ for SMC.

expectedly by far the fastest controller. Then, the standard SMC and NMPC methods as faster controllers than the RK-based ones, which is attributable to the derivative calculations that have been done asynchronously in the RK-based methods. Yet, RK-based methods are fast enough to control a fast system as MagLev.

The methods, PID, standard MPC, RK-MPC, RK-PID and standard SMC, have been compared with respect to control performance (tracking RMSE), robustness, computational complexity and design issues. Based on the comparison results, the following discussions can be made. (i) The experimental results for noiseless case have shown that all methods but PID have exhibited nearly similar control performances. This is due to the fact that the systems to be controlled are all nonlinear, while PID is a linear control method. Moreover, PID method cannot be applied to control the MagLev system since PID is unable to control it in its nonlinear region. When we compare the other methods, it has been observed that RK-based methods have yielded the best control performances. (ii) Similar results have been obtained when we compare the methods with respect to robustness against shot and measurement noises. To sum up, RK-based methods have the

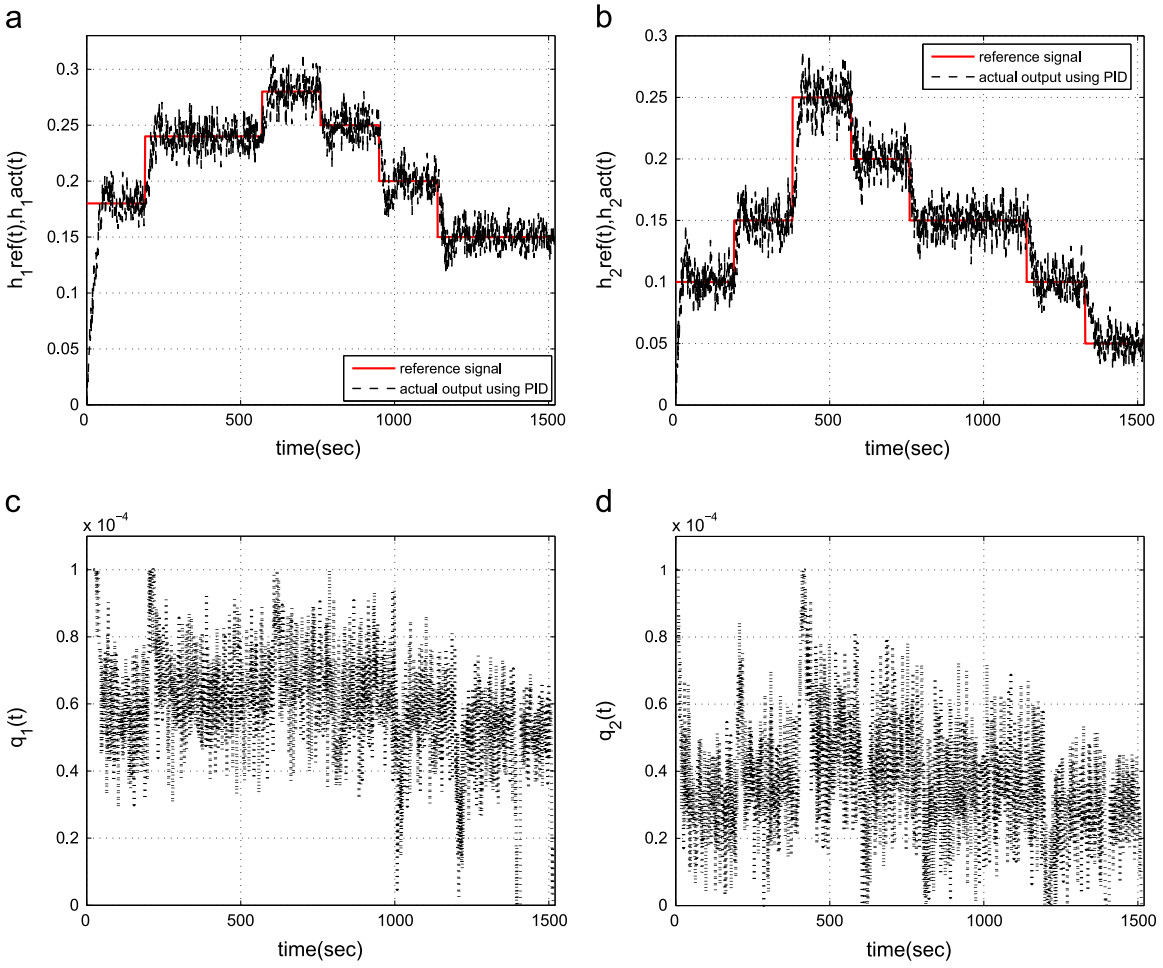

Fig. 13. Real-time experimental results of the liquid-level system for PID (with measurement noise). (a) Liquid-level of $tank_1$, (b) liquid-level of $tank_2$, (c) control signal of $pump_1$, and (d) control signal of $pump_2$.

Table 4
Comparisons with respect to computational time (in ms).

System	PID	SMC	NMPC	RK-MPC	RK-PID
Liquid-level system	0.158	0.1739	2.29	4.574	5.061
MagLev	–	1.681	1.701	2.997	3.518

Table 5
The effect of the design parameters for liquid-level control system (in RMSE).

$\mu=10$, $\lambda=0.01$	$\kappa=5$	$\kappa=10$	$\kappa=20$	$\kappa=25$	$\kappa>25$
$tank_1$	0.0134	0.0121	0.0113	0.0120	Unstable
$tank_2$	0.00961	0.00934	0.00923	0.00926	Unstable
$\kappa=20$, $\lambda=0.01$	$\mu<500$	$\mu=500$	$\mu=1000$	$\mu=2000$	$\mu>2000$
$tank_1$	Unstable	0.0112	0.0113	0.0129	0.0161
$tank_2$	Unstable	0.00925	0.00923	0.00928	0.00941
$\kappa=20$, $\mu=10$	$\lambda<0.00001$	$\lambda=0.001$	$\lambda=0.1$	$\lambda=10$	$\lambda=1000$
$tank_1$	0.0117	0.0113	0.0125	0.011	0.0112
$tank_2$	0.00924	0.00923	0.00923	0.00924	0.00923

best control performances under both noiseless and noisy conditions compared to standard PID, MPC and SMC methods. (iii) The designed methods have been compared with respect to computational complexity. The computational times of the MPC, RK-MPC and RK-PID are much more than those of standard PID and SMC since the former ones have to make the derivative computations at each sampling period, while the latter ones compute the control

Table 6
The effect of the design parameters for MagLev control system (in RMSE).

$\mu=100$, $\lambda=0.06$	$\kappa\leq5$ Unstable	$\kappa=7$ 0.1325	$\kappa=10$ 0.2141	$\kappa\geq13$ Insufficient
$\kappa=7$, $\lambda=0.06$	$\mu=0.1$ 0.1803	$\mu=10$ 0.1627	$\mu=100$ 0.1325	$\mu=1000$ 0.0974
$\kappa=7$, $\mu=100$	$\lambda<0.02$ Insufficient	$\lambda=0.02$ 0.1775	$\lambda=0.06$ 0.1325	$\lambda>0.08$ Unstable

action directly. Still, even the slowest one of the control methods, RK-PID controller can compute the control action less than 5 ms, which is considerably acceptable for many real-time applications. (iv) On the other hand, when we compare the methods by taking their design issues into consideration, it can be stated that the number of design parameters of standard PID and SMC are much more than those of NMPC, RK-MPC and RK-PID especially for the control of MIMO three-tank system.

Based on above discussions, PID controller is not suitable for nonlinear control and SMC can be preferred for nonlinear control when the computational-time is the most important design issue. On the other hand, the MPC-type methods, i.e. NMPC, RK-MPC and RK-PID, are preferable to standard PID and SMC when the control performance under noisy conditions is important, and relatively a less number of design parameters are desired. Among the MPC-type methods, the proposed RK-PID may be the most preferable one since its control performance is better than others and it can

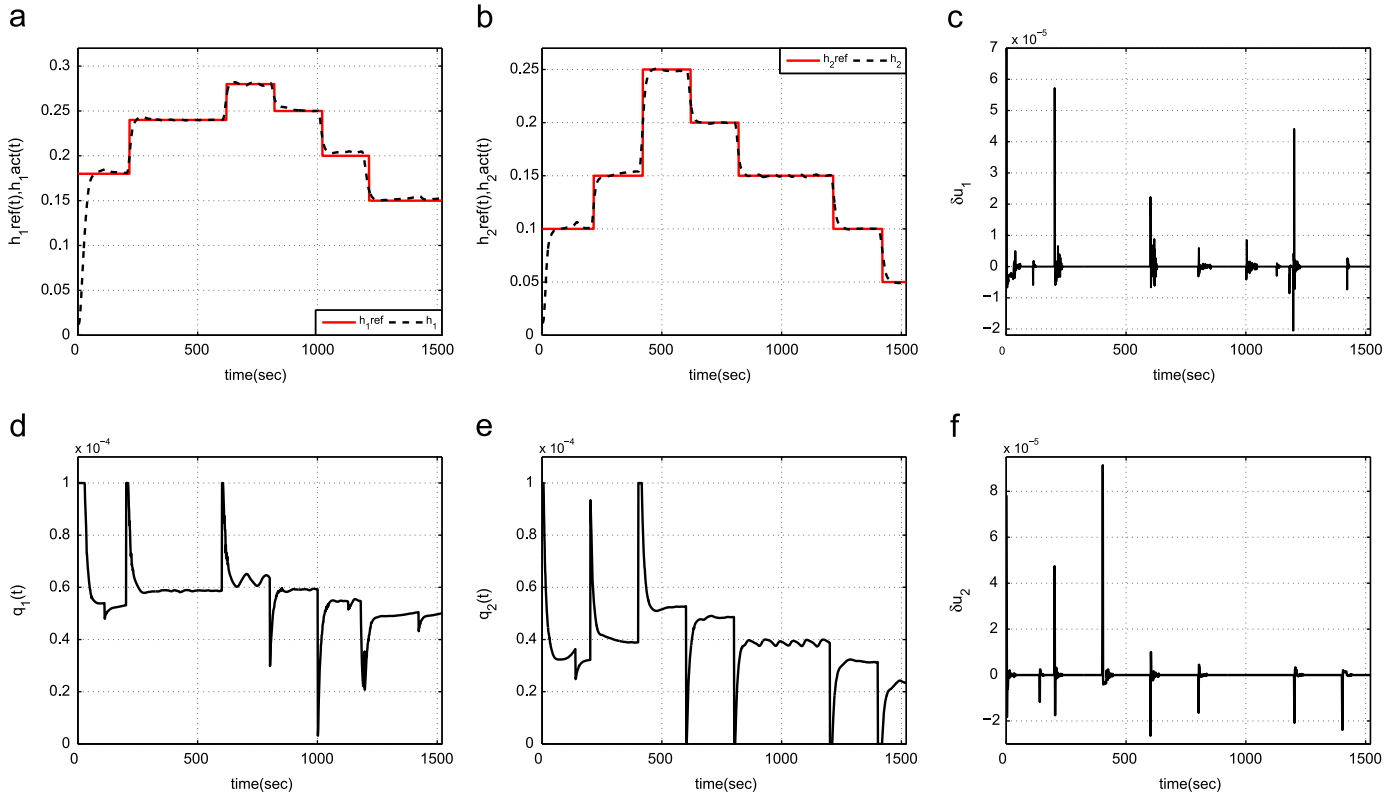

Fig. 14. Real-time experimental results of switched RK-PID for liquid-level system. (a) Liquid-level of $tank_1$, (b) liquid-level of $tank_2$, (c) correction terms of $tank_1$, (d) control signal of $pump_1$, (e) control signal of $pump_2$, and (f) correction terms of $tank_2$.

be used as a single PID controller in its switched mode (which will be explained in Section 4.5), thereby reducing its computational time.

4.4. Sensitivity analysis of the design parameters

The RK-PID structure involves some design parameters such as prediction horizon (κ) and penalty term (λ) which are found by grid search, and switching parameter (μ). In all experimental tests, several triples of κ, λ and μ are applied on the experimental systems to investigate the effects of the parameters on the controller performance. Finally, parameters yielding the best tracking performance are utilized for the proposed RK-PID controller. The choice of κ is important since it affects the system stability. If κ is lower than a critical value, then the RK-PID mechanism cannot perform properly due to the short prediction horizon and thus the PID parameters cannot be tuned correctly, which may lead to instability. Similar observations can be made when κ is upper than another critical value. Moreover, the larger κ values the mechanism has, the higher computational burden and the larger rise time the closed-loop system has. On the other hand, λ penalizes the input slews. As can be observed from Tables 5 and 6, for a stable and slow system (three-tank) the choice of λ do not have a significant effect on the control performance. However, it is very crucial to select a proper λ value for an unstable and fast system (MagLev). The last design parameter in the RK-PID mechanism is μ, which gives a good compromise between a slow and stable direction (Steepest-Descent) and a fast and unstable direction (Gauss-Newton). The lower μ values forces the update algorithm towards Gauss–Newton and leads to some instabilities due to the external disturbances and measurement noises. Thus, as can be seen from the tables, the μ values have been chosen larger than a critical values for each system. More specifically, with regard to selecting appropriate design parameters (κ, λ, μ) for a given system some practical guidelines may be helpful. While selecting the penalty term λ, the terms in the objective function (10) can be used as

$$\lambda \sim \frac{\kappa (y_{max} - y_{min})^2}{(u_{max} - u_{min})^2}, \tag{38}$$

so that the terms are evenly balanced, which complies with the results obtained in our experiments. As far as selection of the prediction horizon (κ) is concerned, it has been observed that a κ value around 10 gives satisfactory results if the sampling period is chosen properly. Finally, selection of the LM parameter μ mostly depends on the existence of some disturbances and noises to the closed loop system. Therefore, to be on the safe side, it is initially chosen large and then the convergence of the PID parameters are observed. If the convergence rate is rather low, then μ can be decreased in order to increase the convergence rate of the parameters and vice versa. This can be carried out by a simple heuristic algorithm within the mechanism.

4.5. Experimental results when RK-PID is switched

In order to test the ability of the PID controller, tuned by RK-PID, the RK-PID mechanism is switched at some time instants during the control based on the switching condition given by

$$P = \frac{\sum_{q=1}^{Q} \sum_{h=1}^{H} (\tilde{y}_q[n-h] - y_q[n-h])^2}{\sum_{q=1}^{Q} \sum_{h=1}^{H} (\tilde{y}[n-h])^2} < \epsilon \tag{39}$$

where $H < \kappa$, and $\epsilon > 0$ is a small scalar. Satisfaction of the condition (39) implies that the correction terms and thus the parameter adaptations are not necessary any more. In this case, the mechanism is switched off and there remains only a fixed PID controller. By doing so, we have an opportunity to observe the control performance of the PID controller tuned by RK-PID.

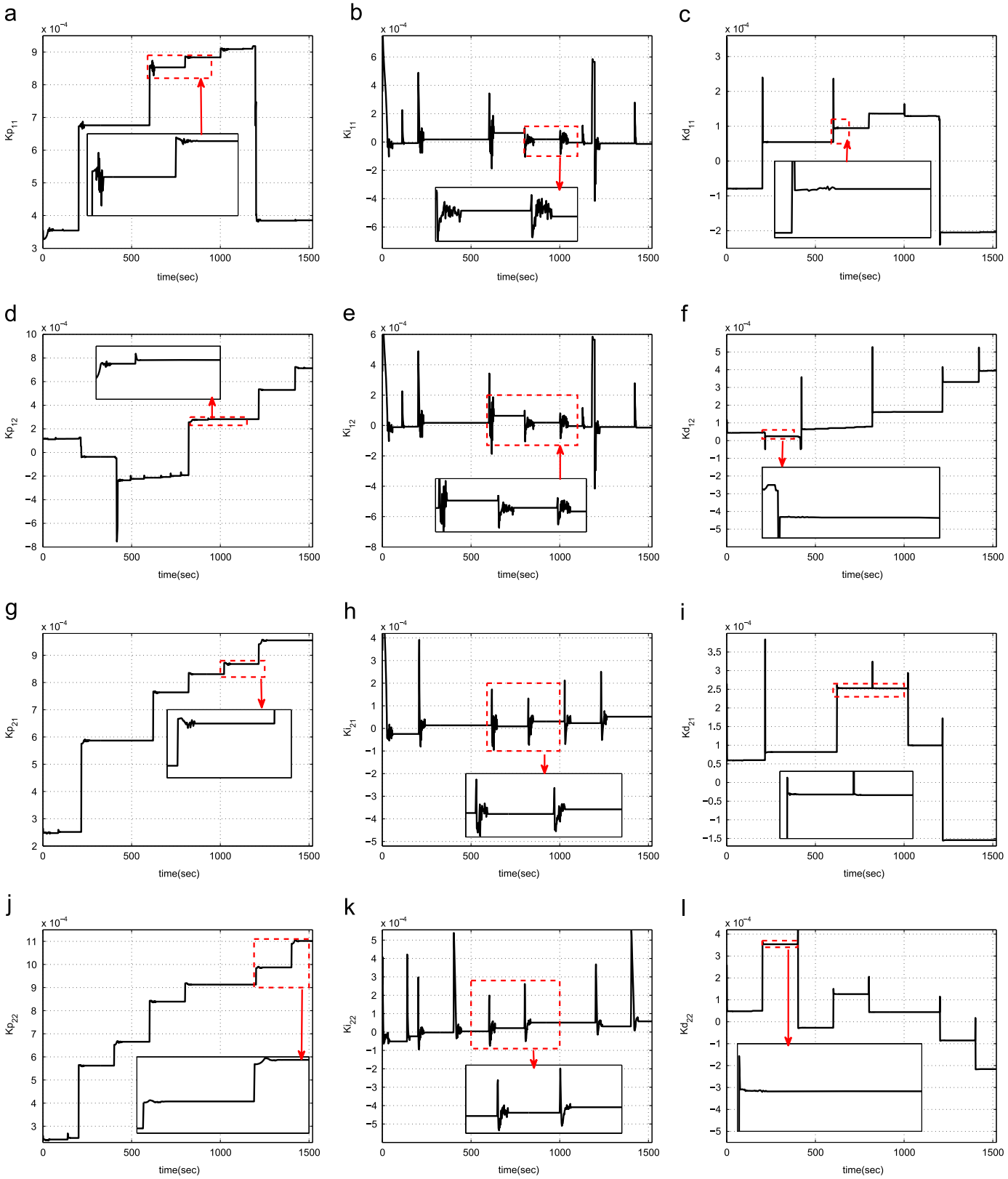

Fig. 15. The PID parameters of the switched RK-PID for liquid-level system. (a) $K_{P_{11}}$, (b) $K_{I_{11}}$, (c) $K_{D_{11}}$ (d) $K_{P_{12}}$, (e) $K_{I_{12}}$, (f) $K_{D_{12}}$, (g) $K_{P_{21}}$, (h) $K_{I_{21}}$, (i) $K_{D_{21}}$, (j) $K_{P_{22}}$, (k) $K_{I_{22}}$, and (l) $K_{D_{22}}$.

Otherwise, if the condition (39) is not hold, then the mechanism remains active and continues to produce the necessary $\Delta\mathbf{K_{PID}}$ and $\delta\mathbf{u}_{n+1}$ terms until the condition is hold. When only the fixed PID, the parameters of which are tuned by RK-PID, is used in the off mode, the computational burden of the controller is reduced dramatically and thus the control action is generated much faster, which constitutes another advantage of the proposed structure.

Figs. 14–16 show the real-time results of the investigated experimental systems for the switched mode of the RK-PID mechanism. It has been observed from the experimental results

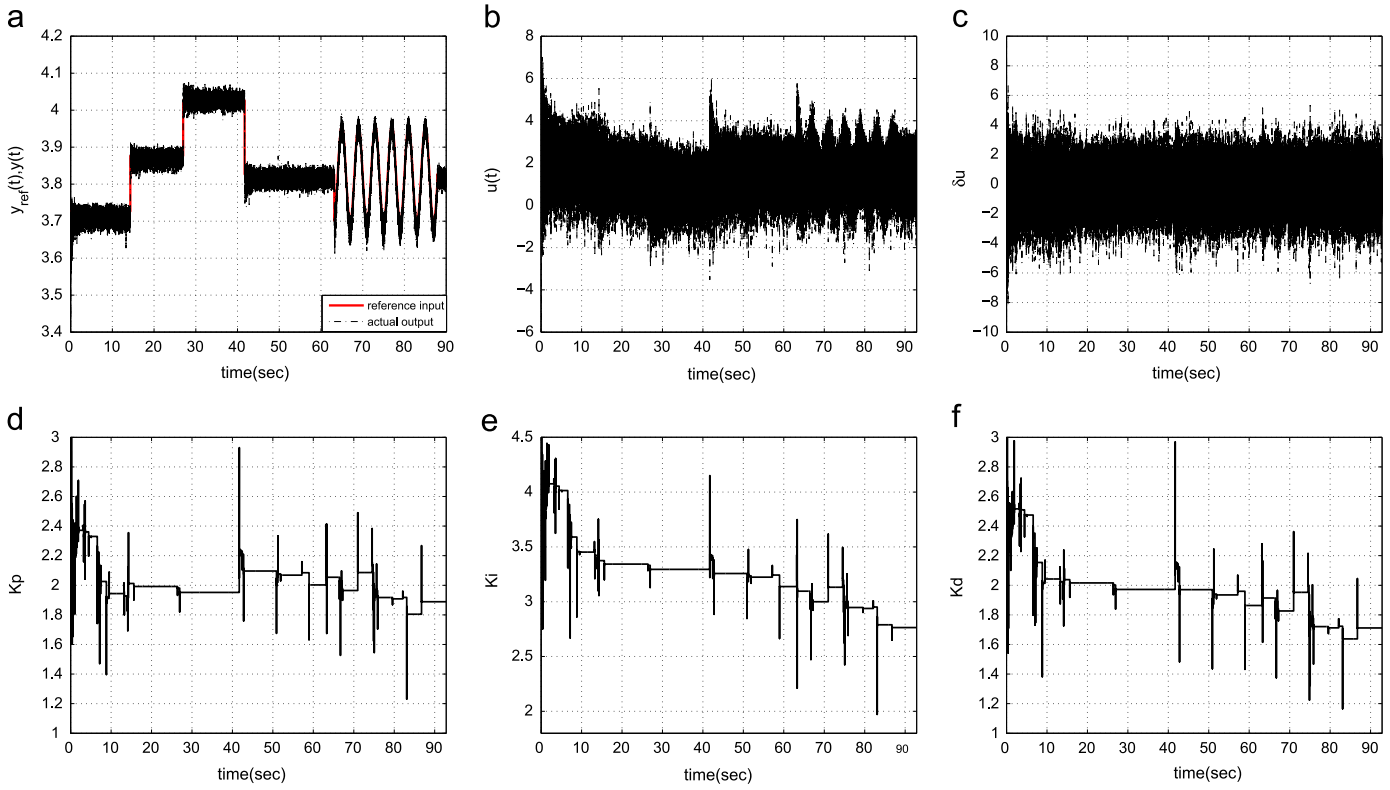

Fig. 16. Real-time experimental results of switched RK-PID for MagLev. (a) Voltage value of the output sensor, (b) control voltage, (c) correction term of the MagLev, (d) K_P, (e) K_I, and (f) K_D.

for the three-tank system that the correction terms get smaller as the PID parameters are tuned and that at a specific time instant the condition (39) is hold and the mechanism is switched off. Accordingly, as can be seen from Fig. 14(c) and (f), the correction terms get closer to zero very fast and the output of the system, controlled by PID, tracks the reference signal very accurately. However, when the reference signal is changed, the PID controller cannot adapt to this change and thus the switching condition is not hold any more and consequently the mechanism is again activated. The time instants when the mechanisms is activated can be seen as the spikes in Fig. 14(c) and (f). Similar observations can be made for the MagLev system with the exception that the mechanism is activated more frequently due to the unstability and high nonlinearities of the system and some fluctuations at the sensor caused by external disturbances.

5. Conclusion

In this study, a novel model-predictive auto-tuning PID controller has been proposed to control nonlinear continuous-time systems. The proposed controller presents a sophisticated auto-tuning mechanism where the PID parameters are tuned using gradient-based adaptation within the MPC framework using RK model of the system. In order to show the efficiency of the proposed controller and compare with some methods in the literature, two real-time experimental systems have been used: one is highly nonlinear, fast and unstable SISO MagLev system and the other one is relatively slow, stable and mild-nonlinear MIMO three-tank liquid-level system.

In the real-time applications, the proposed RK-PID controller, classical PID, NMPC, RK-MPC and standard SMC methods are compared in terms of control performance, robustness, computational complexity and design issues. Following conclusions are drawn from the experimental results. (i) The proposed RK-PID controller provides acceptable control performances such as very small steady-state tracking errors, very short settling time and fast convergence of parameters. (ii) The proposed RK-PID controller is robust against the effects of the external noises, disturbances and changes in the reference trajectory. (iii) Sensitivity analysis for the design parameters has been given experimentally which provides a guideline to design RK-PID for another applications. (iv) The proposed mechanism provides necessary PID parameter adaptations while generating additive correction terms to assist the initially inadequate PID controller. Even though the initial PID parameters are set to zero and thus the PID controller cannot provide necessary control actions, a satisfactory tracking performance is obtained by the additive correction terms generated by the mechanism. (v) The RK-PID controller can be used in switched mode, i.e. when the PID parameters are converged to their ultimate values then the adaptation is stopped, and the RK-PID is used as a fixed PID controller. This mode reduces the computational burden dramatically and produces the control signal much faster.

As a general result, in this paper, a robust, adaptive and predictive PID auto-tuning mechanism (RK-PID) has been introduced. Merits of the proposed mechanism have been experimentally verified on two real-time systems and have been revealed by the comparisons to the standard methods in the literature. Therefore, it is concluded that the RK-PID controller can be used for the control of nonlinear systems to a satisfactory level of performance.

Acknowledgment

This work is partly supported by Pamukkale University Scientific Research Projects Council, Project no. 2012FBE011.

References

[1] Ziegler JG, Nichols NB. Optimum settings for automatic controllers. Trans ASME 1942;64:759–68.
[2] Astrom KJ, Hagglund T, Hang CC, Ho WK. Automatic tuning and adaptation for PID controllers—a survey. Control Eng Pract 1993;1(4):699–714.
[3] Astrom K, Hagglund T. PID controller: theory, design and tuning, 2nd ed. Research Triangle Park: Instrumentation, Systems and Automatic Society; 1995.
[4] Astrom KJ, Hagglund T. Advanced PID control. Research Triangle Park, NC: ISA —The Instrumentation, Systems, and Automation Society; 2006.
[5] Chang WD, Yan JJ. Adaptive robust PID controller design based on a sliding mode for uncertain chaotic systems. Chaos Solitons Fractals 2005;26 (1):167–75.
[6] Parlos AG, Parthasarathy S, Atiya AF. Neuro-predictive process control using on-line controller adaptation. In: IEEE transactions on control systems technology, vol. 9; 2001. p. 741–55.
[7] Cao J, Cao B, Chen W, Xu P. Neural network self-adaptive PID control for driving and regenerative braking of electric vehicle. In: 2007 IEEE international conference on automation and logistics; 2007. p. 2029–34.
[8] Beyhan S, Alci M. Stable modeling based control methods using a new RBF network. ISA Trans 2010;49(4):510–8.
[9] Hong X, Iplikci S, Chen S, Warwick K. A model-based PID controller for Hammerstein systems using B-spline neural networks. Int J Adapt Control Signal, 28(3–5):412–428, http://dx.doi.org/10.1002/acs.2293.
[10] Iplikci S. A comparative study on a novel model-based PID tuning and control mechanism for nonlinear systems. Int J Robust Nonlinear Control 2010;20 (13):1483–501.
[11] Savran A, Kahraman G. A fuzzy model based adaptive PID controller design for nonlinear and uncertain processes. ISA Trans 2014;53(2):280–8.
[12] Rongrong S, Weihua M, Zili C. Study on improved fuzzy immune PID controller for maglev transportation system with track irregularity. In: Applied mechanics and materials, vol. 423; 2013. p. 2825–31.
[13] Junior GFB, Barreiros JAL. PID control design for a Maglev train system. In: Applied mechanics and materials, vol. 389; 2013. p. 425–9.
[14] Moreno Valenzuela J, Santibez V. Robust saturated PI joint velocity control for robot manipulators. Asian J Control 2013;15(1):64–79.
[15] Santibanez V, Camarillo K, Moreno-Valenzuela J, Campa R. A practical PID regulator with bounded torques for robot manipulators. Int J Control Autom Syst 2010;8(3):544–55.
[16] Su Y, Muller PC, Zheng C. Global asymptotic saturated PID control for robot manipulators. IEEE Trans Control Syst Technol 2010;18(6):1280–8.
[17] Duan XG, Deng H, Li HXA. Saturation-based tuning method for fuzzy PID controller. IEEE Trans Ind Electron 2013;60(11):5177–85.
[18] Clarke DW, Mohtadi C, Tuffs PS. Generalized predictive control Part I. The basic algorithm. Automatica 1987;23(2):137–48.
[19] Rawlings JB. Tutorial overview of model predictive control. IEEE Control Syst 2000;20(3):38–52.
[20] Maciejowski JM. Predictive control with constraints, Prentice Hall international ed.; 2002.
[21] Camacho EF, Alba CB. Model predictive control. Springer; 2004.
[22] Miller RM, Shah SL, Wood RK, Kwok EK. Predictive PID. ISA Trans 1999;38 (1):11–23.
[23] Moradi MH, Katebi MR, Johnson MA. Predictive PID control: a new algorithm. In: IECON '01. 2001 The 27th annual conference of the IEEE industrial electronics society, vol. 1; 2001. p. 764–9.
[24] Na MG, Auto-tuned PID. controller using a model predictive control method for the steam generator water level. IEEE Trans Nucl Sci 2001;48(5):1664–71.
[25] Xu M, Li S, Qi C, Cai W. Auto-tuning of PID controller parameters with supervised receding horizon optimization. ISA Trans 2005;44(4):491–500.
[26] Zhang R, Wu S, Lu R, Gao F. Predictive control optimization based PID control for temperature in an industrial surfactant reactor. Chemom Intell Lab Syst 2014;135:48–62.
[27] De Keyser R, Donald I James. Application of the NEPSAC nonlinear predictive control strategy to a semiconductor reactor. In: Assessment and future directions of nonlinear model predictive control; 2007. p. 503–12.
[28] Lu J, Chen G, Ying H. Predictive fuzzy PID control: theory, design and simulation. Inf Sci 2001;137(4):157–87.
[29] Iplikci S. Runge–Kutta model-based adaptive predictive control mechanism for non-linear processes. Trans Inst Meas Control 2013;35(2):166–80.
[30] Beyhan S. Runge–Kutta model-based nonlinear observer for synchronization and control of chaotic systems. ISA Trans 2013;52(4):501–9.
[31] Burrage K, Butcher JC. Non-linear stability of a general class of differential equation methods. BIT Numer Math 1980;20(2):185–203.
[32] Cooper GJ. Stability of Runge–Kutta methods for trajectory problems. IMA J Numer Anal 1987;7(1):1–13.
[33] Zeltom. Electromagnetic levitation system. Zeltom LLC., 2013.
[34] Amira. DTS 200 laboratory setup three-tank-system. Amira GmbH, Duisburg; 2002.
[35] Iplikci S. A support vector machine based control application to the experimental three-tank system. ISA Trans 2010;49(3):376–86.
[36] Plucenio A, Pagano JD, Bruciapaglia HA, Normey-Rico EJ. A practical approach to predictive control for nonlinear processes. In: 7th IFAC symposium on nonlinear control systems (2007), vol. 7; 2008. p. 210–5.
[37] Slotine JJE, Li W. Applied nonlinear control. NJ: Prentice-Hall Englewood Cliffs; 1991.
[38] Benamor A, Chrifi-Alaui L, Messaoud H, Chaabane M. Sliding mode control, with integrator, for a class of MIMO nonlinear systems. Engineering 2011;3 (05):435.